Completion of neural crest cell production and emigration is regulated by retinoic acid-dependent inhibition of BMP signaling

Dina Rekler and Chaya Kalcheim,*

Department of Medical Neurobiology, Institute of Medical Research Israel-Canada (IMRIC) and the Edmond and Lily Safra Center for Brain Sciences (ELSC).

Hebrew University of Jerusalem-Hadassah Medical School

Jerusalem 9112102, P.O.Box 12272, Israel

Emails: Dina Rekler, dina.rekler@mail.huji.ac.il; Chaya Kalcheim, kalcheim@cc.huji.ac.il

*To whom correspondence should be addressed.

Running title: Local RA signals the end of neural crest production

Key words: BAMBI, cell specification, dorsal interneurons, Foxd3, Hairy, neural tube, Raldh2, Roof plate, Snai2, Sox9.

Abstract

Production and emigration of neural crest cells is a transient process followed by the emergence of the definitive roof plate. The mechanisms regulating the end of neural crest ontogeny are poorly understood. Whereas early crest development is stimulated by mesoderm-derived retinoic acid, we report that the end of the neural crest period is regulated by retinoic acid synthesized in the dorsal neural tube. Inhibition of retinoic acid signaling in the neural tube prevents the normal upregulation of BMP inhibitors in the nascent roof plate and prolongs the period of BMP responsiveness which otherwise ceases close to roof plate establishment. Consequently, neural crest production and emigration are extended well into the roof plate stage. In turn, extending the activity of neural crest-specific genes inhibits the onset of retinoic acid synthesis in roof plate suggesting a mutual repressive interaction between neural crest and roof plate traits. Although several roof plate-specific genes are normally expressed in the absence of retinoic acid signaling, roof plate and crest markers are co-expressed in single cells and this domain also contains dorsal interneurons. Hence, the cellular and molecular architecture of the roof plate is compromised. Collectively, our results demonstrate that neural tube-derived retinoic acid, via inhibition of BMP signaling, is an essential factor responsible for the end of neural crest generation and the proper segregation of dorsal neural lineages.

Introduction

The generation of cell type diversity during normal development takes place in a stereotypic sequence and a spatially regulated manner (Holguera and Desplan, 2018; Kohwi and Doe, 2013). An example of such a precision is the development of the central and peripheral subdivisions of the nervous system (CNS and PNS), that arise from a common domain in the dorsal neural tube (NT). This domain sequentially generates neural crest cells (NC), progenitors of the peripheral nervous system (PNS)(Bronner, 2012; Le Douarin and Kalcheim, 1999), followed by the definitive roof plate (RP) of the CNS, which is flanked ventrally by dorsal interneuron populations (Andrews et al., 2019; Chizhikov and Millen, 2005; Helms and Johnson, 2003; Kalcheim and Kumar, 2017; Krispin et al., 2010a; Nitzan et al., 2016).

At trunk levels of the avian axis, NC progenitors sequentially emigrate from the NT for a period of about two days while actively proliferating before and after delamination and largely synchronizing to the S-phase of the cell cycle during the emigration event (Burstyn-Cohen and Kalcheim, 2002). Lineage tracing experiments showed that RP progenitors originate ventral to the cohort of premigratory NC (Krispin et al., 2010b). As a result of continuous cell emigration, RP precursors undergo a ventro-dorsal shift and, upon completion of NC departure, they reach the dorsal midline of the NT and form the definitive RP (Krispin et al., 2010b). RP progenitors gradually exit the cell cycle to become post-mitotic (Kahane and Kalcheim, 1998), and function primarily as a dorsal organizer, providing a gradient of Bone Morphogenetic Protein (BMP) and Wnt activity which is crucial for development of dorsal interneurons (Chizhikov and Millen, 2005; Le Dréau and Martí, 2013; Muroyama et al., 2002; Zechner et al., 2007) and for proliferation of ependymal cells at later stages (Shinozuka et al., 2019; Xing et al., 2018).

Many aspects of early NC ontogeny were extensively studied, from induction to specification,

59 epithelial to mesenchymal transition (EMT) and emigration. Yet, virtually nothing is known
60 about the mechanisms underlying the end of NC production and transition to definitive RP
61 (Rekler and Kalcheim, 2021).
62
63 BMP has been found to regulate several aspects of NC development. In the early neurula, BMP
64 is derived from the non-neural ectoderm and participates in NC induction at the neural plate
65 border (Endo et al., 2003). Upon closure of the NT, cells of the dorsal domain synthesize and
66 secrete BMP, which acts in a graded rostro-caudal fashion to activate Wnt signaling and a
67 network of downstream genes that altogether promote NC EMT and emigration [Reviewed in
68 (Kalcheim, 2018; Theveneau and Mayor, 2012a)].

69 A first step towards understanding the segregation between NC and RP, was the finding that
70 approaching the end of the NC production in the avian embryo, the dorsal NT becomes
71 insensitive to BMP, even though this factor continues to be produced by nascent RP cells. This
72 suggested that local downregulation of BMP signaling is necessary for the end of NC stage, a
73 conclusion further illustrated by a premature cessation of NC proliferation and delamination
74 upon early inhibition of BMP signaling (Nitzan et al., 2016). These events were mediated by
75 the transcription factor HES1/Hairy1, as early misexpression of *hes1/hairy1* in the dorsal NT
76 led to a downregulation of the *Alk3* BMP receptor and of pSmad activity (Nitzan et al., 2016).

77 However, the factors that orchestrate these BMP-dependent processes, leading to cessation of
78 NC production, segregation of NC and RP lineages, and formation of the definitive RP, remain
79 unknown. Along this line, whether cessation of NC production and RP development are
80 regulated by the same or by independent mechanisms is yet to be elucidated.

81 A recent RNA-seq analysis revealed transcriptional heterogeneity between premigratory NC
82 and definitive RP cells, uncovering a set of genes expressed specifically at the onset of the RP

83 stage (Ofek et al., 2021). One of these genes is *Raldh2/Aldh1a2*, that encodes an enzyme
84 responsible for the biosynthesis of the morphogen retinoic acid (RA) (Haselbeck et al., 1999),
85 central to multiple neurodevelopmental processes (Diez del Corral and Morales, 2014; Lara-
86 Ramírez et al., 2013; Wilson et al., 2004). RA derived from the *Raldh2*-expressing somitic
87 mesoderm has been described as a key factor in NT development, including control of
88 motoneuron specification (Novitch et al., 2003; Wilson et al., 2004) and initiation but not
89 maintenance of NC EMT and emigration (Martinez-Morales et al., 2011). Although expression
90 of *Raldh2* in the dorsal NT was previously reported (Berggren et al., 1999; Blentic et al., 2003),
91 its precise temporal dynamics vis-à-vis NC/RP phases and function/s have not been
92 characterized. Hence, the discovery of local RA production in the dorsal NT only by the end
93 of the NC stage prompted us to hypothesize a role for RA in events concerning the late NC.

94 In this study, we unravel a fundamental role of dorsal NT-derived RA in controlling the end of
95 NC production. Using two separate tools to inhibit RA signaling in the quail embryo, we
96 demonstrate that RA is responsible for downregulation of BMP signaling in the dorsal NT. In
97 the absence of RA signaling, cells in the dorsal NT retain expression of NC markers well into
98 the RP stage which also displays additional NC traits such as a high mitotic rate and impaired
99 epithelial properties. Furthermore, we show that lack of RA signaling prolongs cell
100 delamination into the RP stage. The latter effect is abrogated by concomitant inhibition of BMP
101 signaling, suggesting that, the RA-dependent extension of NC EMT is also mediated by BMP.
102 Whereas RA signaling represses expression of NC genes such as *foxd3, snai2* and *sox9*,
103 extending the activity of the latter beyond the NC stage inhibits transcription of *Raldh2* in the
104 RP, suggesting that NC and RP traits stand in a mutual cross-repressive interaction.
105 Remarkably, maintenance of NC traits in the dorsal NT does not prevent the advent of RP
106 traits, or RP-dependent specification of dorsal interneurons. Rather, in the absence of RA

activity, the spatial and temporal segregation of dorsal lineages, as well as the structural integrity of this signaling center, are compromised.

110 **Results**

111 **RA is both produced and active in the nascent RP**

112 The spatio-temporal dynamics of RA, including synthesis, degradation and activity, was
113 examined in the trunk of quail embryos from stages corresponding to NC production until
114 formation of the nascent RP. RA is produced from retinol via two consecutive reactions: first,
115 retinol is converted to retinaldehyde by RDH enzymes, then it is oxidized to RA by
116 RALDH/ALDH1; additionally, CYP1B1 catalyzes both reactions [Fig. 1A and (Chambers et
117 al., 2007; Kam et al., 2012; Reijntjes et al., 2005; Rhinn and Dollé, 2012). Of the three known
118 RALDH-encoding genes, only *Raldh2* is expressed in the avian trunk at these developmental
119 stages (Blentic et al., 2003). At an early NC stage, *Raldh2* was expressed in the intermediate
120 and paraxial somitic mesoderm but not in the neuroepithelium (Fig. 1B). At an advanced NC
121 stage, *Raldh2* continued to be transcribed in subdomains of the somite-derived sclerotome and
122 dermomyotome (Fig. 1C) and was weakly detected in the dorsal NT (Fig. 1C, arrowhead).
123 Subsequently, *Raldh2* was strongly expressed in the nascent RP itself (Fig. 1D, arrowhead,
124 Fig.1 Supp.1A). In contrast, no expression of *Cyp1B1* was apparent in the NT at any stage,
125 although robust transcription was evident in the paraxial mesoderm throughout development
126 (Fig. 1E-G).

127 RA is degraded by CYP26 enzymes of the cytochrome P450 family. *Cyp26A1* is the only
128 member of the family to be expressed in the avian trunk at early stages of nervous system
129 development (Blentic et al., 2003). At an early NC stage, *Cyp26A1* was absent from the NT
130 and adjacent mesoderm, it was later detected in a salt and pepper pattern in dorsal interneuron
131 progenitors, but was excluded from the dorsal midline (Fig. 1H-I). As the definitive RP formed,
132 it was also occasionally detected in RP cells (Fig. 1J).

133 CRABP1 is a carrier protein of RA, which participates in regulation of RA function and/or
134 metabolism (Maden et al., 1989; Venepally et al., 1996). At the early NC stage there was no
135 prominent expression of *CRABP1* in either the NT or paraxial mesoderm (Fig. 1K); at an
136 advanced NC stage it appeared in the basal domain of the NT, corresponding to the positions
137 adopted by differentiating neurons, yet absent from the dorsal and ventral midline regions (Fig.
138 1L). At the RP stage *CRABP1* was additionally expressed in two stripes at the lateral domain
139 of the RP [(Fig. 1M, Supp.1A, and see (Ofek et al., 2021)].

140 Next, we examined expression of RA receptors. RA acts by binding to a heterodimer of nuclear
141 receptors, RAR and RXR, each of which is encoded by three genetic variants. Expression of
142 all RA receptors was predominantly ubiquitous in both early NC (Diez del Corral et al., 2003)
143 and RP stages with at least one variant of each subunit expressed in the dorsal NT at the nascent
144 RP stage (RARα, RARβ and RXRγ, but not RARγ or RXRα) (Fig. 1 Supp. 2). This suggests
145 that RA acts during the transition into the nascent RP where a tight regulation of local RA
146 levels may take place.

147 To directly examine the activity of RA in the dorsal NT, we electroporated a destabilized GFP
148 plasmid driven by a retinoic acid response element (RARE-d2EGFP) at E2.5 and analyzed GFP
149 fluorescence 12 and 48 hours later, at NC and RP stages, respectively. Whereas control RFP
150 was apparent throughout the dorso-ventral extent of the NTs, RARE activity was primarily
151 present within the dorsal half of the NT at both stages (Fig. 1N-O').

152 Together, these data show that whereas NC cells respond to mesoderm-derived RA (see
153 Introduction for refs.), but do not synthesize it, the emerging RP both synthesizes and responds
154 to this factor. Hence during the transition from NC to definitive RP, the latter becomes a local
155 source of RA. This prompted us to hypothesize that locally produced RA plays a role in either

156 the end of NC production and emigration, in the ensuing formation of the RP, or in both
157 processes.
158

Figure 1

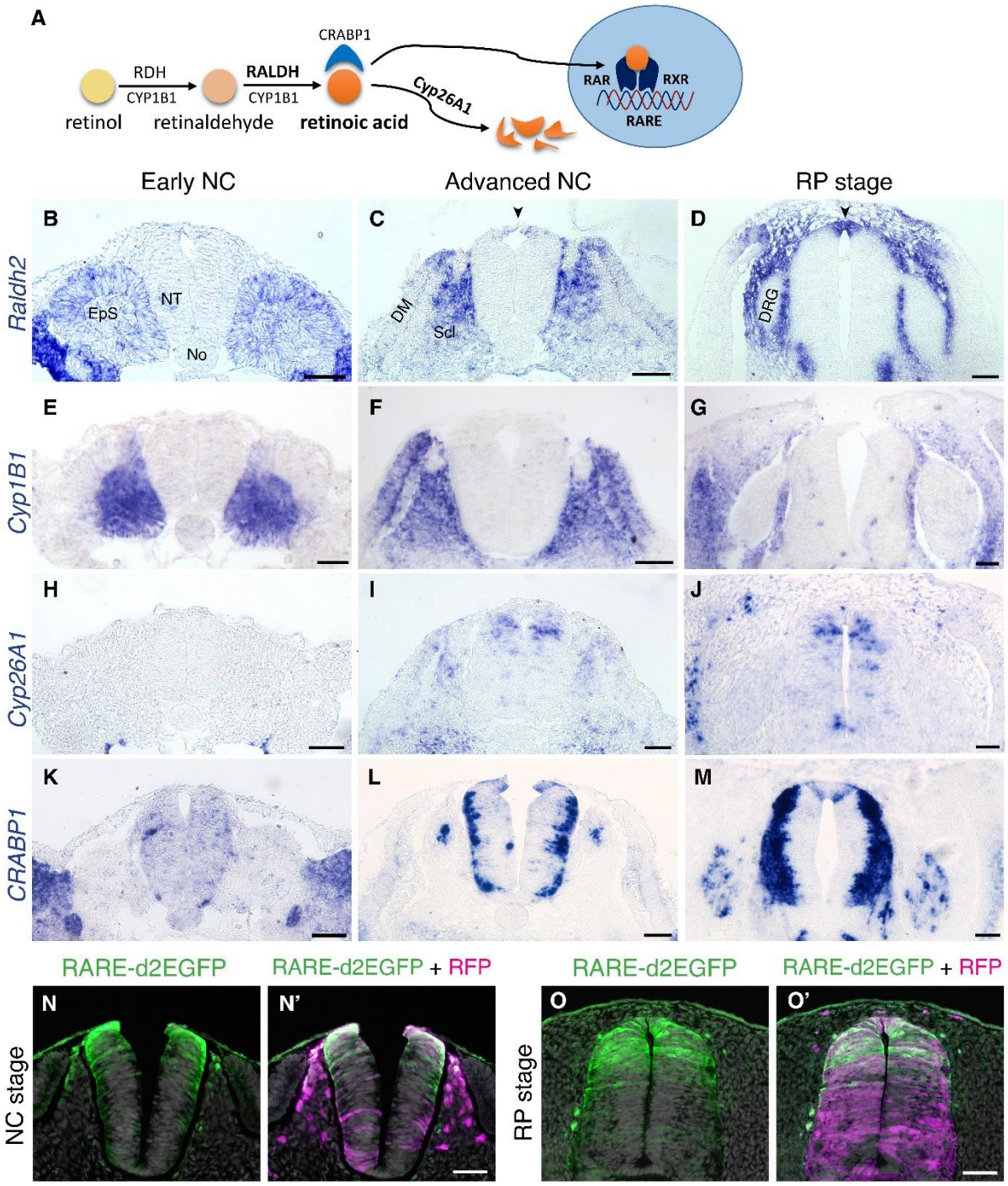

Figure 1- RA is both produced and active in the nascent RP

(A) Schematic illustration of the metabolic and signaling pathways of RA.

(B-M) Expression patterns of genes participating in RA synthesis and metabolism, both at early and advanced NC stages [E2 (27 ss) and E3 (35 ss), respectively], and at the RP stage (E4). ISH for *Raldh2/Aldh1a2* (B-D), *Cyp1B1* (E-G), *Cyp26A1* (H-J) and *CRABP1* (K-M). Images were taken at the level of somites 25-27.

166 (N-O') RA activity in the NT at NC and RP stages, indicated by the presence of destabilized GFP
167 (d2EGFP) driven under the control of a RARE element. Embryos were electroporated at E2.5 (28 ss)
168 along with control RFP to monitor efficiency of transfection, and analyzed 12 hours (N-N', at 35 ss) or
169 48 hours (O-O', at E4) later. RARE activity was evident in the dorsal NT of NC-stage embryos (N=8/8),
170 and RP-stage embryos (N=7/7). Images were taken at the level of somites 25-27.

171 Abbreviations, EpS, epithelial somite, No, notochord, NT, neural tube, DM, dermomyotome, Scl,
172 sclerotome, DRG, dorsal root ganglion. Scale bar, 50 μm.

173

174 **RA is responsible for the loss of sensitivity of dorsal NT progenitors to BMP during the**
175 **transition from NC to RP**

176 In previous studies, we showed that BMP signaling is essential for NC EMT and emigration
177 (Sela-Donenfeld and Kalcheim, 1999). Subsequently, when approaching the RP stage,
178 although BMP is still produced by the nascent RP, the latter becomes refractory to it, likely
179 via downregulation of BMP receptor 1A (*Alk3*), and upregulation of BMP inhibitory genes
180 (Fig.1 Supp.1B) (Nitzan et al., 2016; Ofek et al., 2021). The onset of *Raldh2* synthesis close to
181 RP development prompted us to hypothesize that RA, locally produced in the dorsal NT,
182 regulates this dynamic cellular behavior vis-a-vis BMP. To this end, we implemented two
183 independent means to inhibit RA activity *in vivo*: 1) RARα403 - a truncated human RA
184 receptor that lacks the transactivation domain and therefore acts in a dominant-negative fashion
185 (Gupta and Sen, 2015) , and 2) Cyp26A1 which encodes a RA-degrading enzyme.

186 First, the efficacy of these constructs was tested by co-electroporation with RARE-RFP. RFP
187 intensity was significantly reduced by 79% and 88% in Cyp26A1- and RARα403-
188 electroporated embryos, respectively, when compared to GFP-only controls. Similarly,
189 RARα403 almost completely abolished the RARE-AP signal observed in controls (Fig.2 Supp.
190 1). Thus, both RARα403 and Cyp26A1 can be effectively used to examine the consequences
191 of RA signaling inhibition.

192 Next, we investigated the effect of RA on the dynamics of BMP signaling. First, we monitored
193 pSmad 1/5/9 expression, a readout of BMP activity, at the NC stage. Control GFP was
194 delivered to embryos aged 27 somite pairs followed by fixation 12 hours later. pSmad was
195 strongly expressed in the dorsal NT (Fig. 2A,A'), corroborating previous findings (Nitzan et
196 al., 2016). In parallel, NTs were electroporated at E2.5 (27 somite pairs at the level of epithelial
197 somites, NC stage) with either RARα403 or Cyp26A1 and analyzed 2 days later (E4, RP stage).

198 As expected (Nitzan et al., 2016), the RP of control embryos was already devoid of BMP
199 activity at this stage (Fig. 2B,B', arrows). In contrast, the RP domain of embryos treated with
200 either RARα403 or Cyp26A1 was pSmad-positive, indicating a failure to normally
201 downregulate BMP signaling (Fig. 2C-D', arrowheads). The dI1 progenitor population of
202 dorsal interneurons, located ventral to the RP, was also pSmad-positive, consistent with its
203 dependency on BMP for proper development (Duval et al., 2019; Lee et al., 1998; Tozer et al.,
204 2013; Wine-Lee et al., 2004). Quantification of pSmad intensity confirmed a significant
205 increase in Cyp26A1 and RARα403-treated embryos compared to controls. This was apparent
206 even if measurement of pSmad intensity comprised the dorsal NT from its midline to the ventral
207 border of pSmad^{+} staining, that included dI1 progenitors (Fig. 2E). These results show that
208 inhibition of RA signaling extends BMP activity into the RP stage by preventing its normal
209 downregulation during the transition from NC to RP.

210 We next examined whether the observed RA-dependent downregulation of BMP activity is
211 mediated by a corresponding upregulation of BMP inhibitors at the RP stage. In this context,
212 Hairy1 was previously reported to act as a specific RP-derived BMP inhibitor thus participating
213 in the end of NC production (Nitzan et al., 2016). Furthermore *hairy1/qHes4*, and the known
214 BMP inhibitors *BAMBI* (Brazil et al., 2015) and *Grem1* (Sun et al., 2006), were unraveled as
215 specific RP markers in a recent RNA-seq analysis comparing dorsal NT cells at both
216 premigratory NC and RP stages (Fig.1 Supp.1B) (Ofek et al., 2021). Embryos electroporated
217 with either Cyp26A1 or RARα403 at E2.5 exhibited a substantially decreased intensity of
218 *BAMBI* mRNA staining in the RP relative to controls (Fig. 2F-I). Similarly, RARα403
219 significantly affected the upregulation of both *hairy1* and *Grem1* in RP when compared to
220 control embryos (Fig. 2J-O). These results show that the downregulation of BMP signaling by
221 RA is accounted for, at least partially, by upregulation of BMP inhibitory genes.

222 In a previous study, we reported that BMP-dependent emigration of NC cells is mediated by
223 Wnt activity (Burstyn-Cohen et al., 2004). A dynamic behavior of Wnt pathway genes between
224 NC and RP stages was also evident in a RNA-seq analysis (Fig.1 Supp.1C). This raised the
225 possibility that, in the absence of RA, extended BMP signaling at the RP stage would be
226 associated with enhanced Wnt activity. To this end, we assessed Wnt signaling in NC and RP
227 by electroporating a destabilized Wnt reporter, 12XTopFlashd2GFP, together with control
228 RFP. Whereas significant activity of the Wnt pathway was observed in the early dorsal NT and
229 emigrating NC cells, a substantial decrease in 12XTopFlashd2GFP expression was apparent in
230 the normal RP (Fig.2 Supp. 2A-B', D). In contrast, a significantly enhanced expression was
231 measured in the RP of RARα403-transfected NTs (Fig.2 Supp.2C-D). These results show that
232 inhibition of RA signaling extends Wnt activity into the RP stage by preventing its normal
233 downregulation during the transition from NC to RP. Hence, RA is necessary for the
234 downregulation of BMP and of downstream Wnt signaling towards ending NC production
235 and/or emigration.

236

237

Figure 2

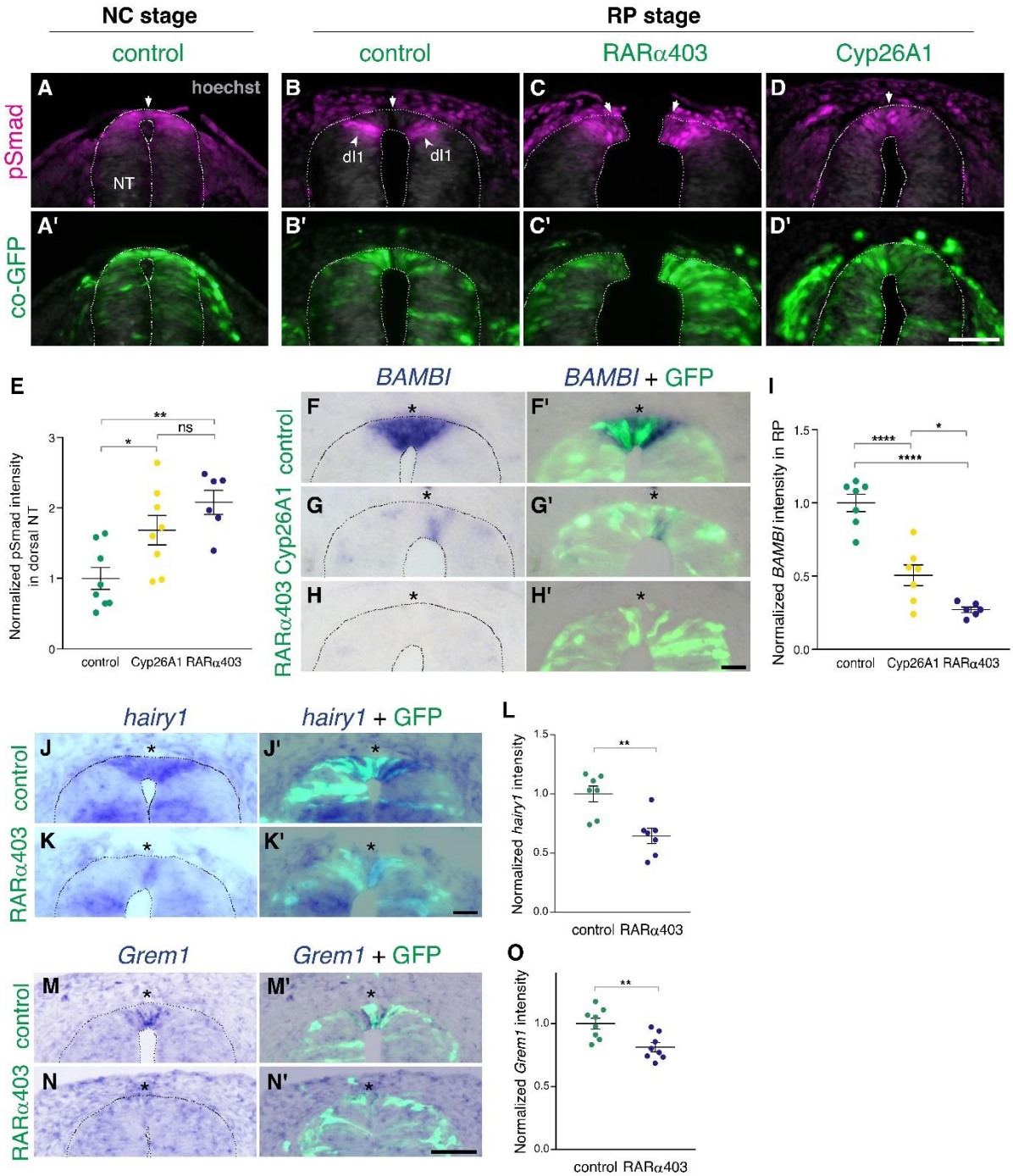

Figure 2- RA is responsible for the loss of sensitivity of dorsal NT progenitors to BMP during the transition from NC to RP.

(A-D') Immunostaining for pSmad1/5/9. Embryos at E2.5 (27-8ss) were co-electroporated with RARα403, Cyp26A1 or with a control PCAGG vector, along with GFP, and analyzed at 35ss (control only, NC stage) and at E4. Note the presence of BMP activity in premigratory NC (A) and its absence in the RP of control embryos (N=8, B-B'). Whereas only ventrally located dorsal interneurons are positive in control embryos, the RP domain itself is positive in Cyp26A1 (N=8) and RARα403-electroporated embryos (N=7, C-C',D-D'). (E) Quantification of pSmad staining intensity (measured

247 area includes dorsal interneurons). Imaging and quantification were performed at somite levels 24-26.
248 Four-to-21 sections per embryo were analyzed. *p < 0.05, **p < 0.005 , one-way ANOVA with post-
249 hoc Tukey's tests.

250 (F-O) In-situ hybridization of embryos electroporated with Cyp26a1 or RARα403 at E2.5 (27 ss) and
251 analyzed at E4. Asterisks mark the RP domain.

252 (F-I) ISH for *BAMBI*, showing downregulation in the RP of Cyp26A1- and RARα403-treated embryos.
253 (I) For quantification of the intensity of *BAMBI*, 6-to-21 sections per embryo were analyzed at somite
254 levels 24-26. N = 7,7 and 6 embryos for control, Cyp26A1 and RARα403, respectively. *p < 0.05,
255 ****p < 0.0001, one-way ANOVA with post-hoc Tukey's tests.

256 (J-L) ISH for *hairy1*, showing downregulation in the RP of RARα403-treated embryos. (L) For
257 quantification of the intensity of *hairy1,* 7-18 sections per embryo were analyzed at somite levels 24-
258 26. N = 7 embryos for each group. **p < 0.005, Student's unpaired t-test.

259 (M-O) ISH for *Grem1*, showing downregulation in the RP of RARα403-treated embryos. For
260 quantification of the intensity of *Grem1*, 11-27 sections per embryo were analyzed at somite levels
261 24-26. N= 8 embryos for each group. **p < 0.005 via Student's unpaired t-test. Abbreviations, dI1,
262 dorsal interneurons 1, RP, roof plate. Scale bar, 50 μm.

263

264 **RA downregulates NC markers during the transition to definitive RP**

265 Our results prompted us to investigate whether the observed persistence of BMP and Wnt
266 activities into the RP stage is associated with a retention of NC identity.

267 *Foxd3*, *snai2* and *sox9* are known premigratory markers of trunk NC cells (Nieto et al., 1994;
268 Sela-Donenfeld and Kalcheim, 1999), and are downregulated in the dorsal NT upon emigration
269 of neural progenitors, being absent from prospective melanoblasts and RP (Krispin et al.,
270 2010b; Nitzan et al., 2012; Ofek et al., 2021). Expression of *foxd3*, *snai2* and *sox9* transcripts
271 was examined at the RP stage in embryos electroporated with RARα403. Strikingly, whereas
272 no mRNA expression was detected in controls, all three genes persisted in the dorsal NT of
273 treated embryos (Fig. 3A-F', arrowheads). Moreover, using immunohistochemistry to assess
274 Sox9 protein, we confirmed its maintenance in the dorsal NT at the RP stage both in Cyp26A1-
275 and RARα403-electroporated embryos (Fig. 3G-J).

276 These findings suggest that endogenous RA signaling underlies the loss of NC identity towards
277 the end of the NC period.

278

Figure 3

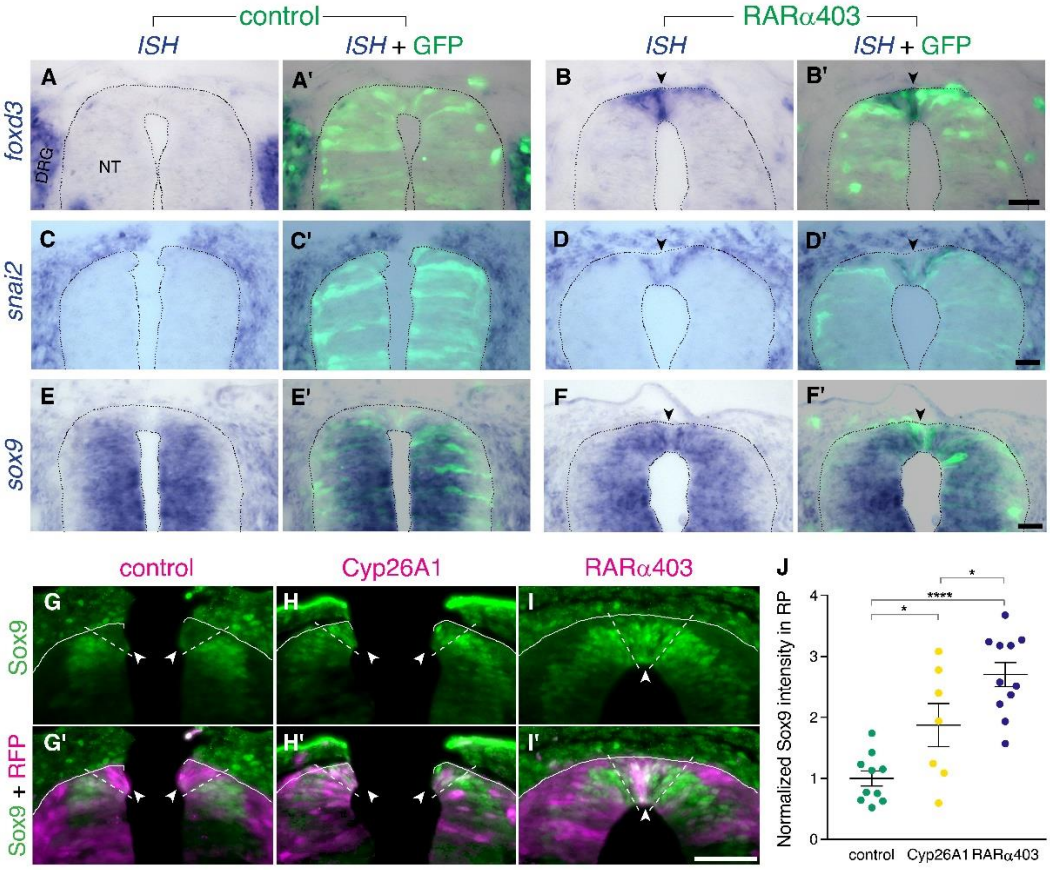

Figure 3- RA downregulates NC markers during the transition to definitive RP

(A-F') ISH for neural crest markers on embryos electroporated with GFP along with control PCAGG or RARα403 at E2.5 (27ss) and analyzed at E4. Arrowheads point to the RP in RARα403-treated embryos. (A-B') ISH for *foxd3*, showing no expression in the RP of control embryos (N= 7) compared to strong expression in the RP of all RARα403-treated embryos (N = 7). (C-D') ISH for *snai2*, showing no expression in the RP of control embryos (N = 11) and clear expression in the RP of all RARα403-treated embryos (N = 11). (E-F) ISH for *sox9*, showing no expression in the RP of control embryos (N = 9) and strong expression in the RP of all RARα403-treated embryos (N = 9). Note as well expression of *sox9* mRNA in more ventral regions of the NT and in adjacent sclerotome. Imaging and analysis were performed at somite levels 25-27.

(G-J) Immunostaining for Sox9 in control and experimental embryos, showing the presence of Sox9 protein in the RP of Cyp26A1- and RARα403-treated embryos (arrowheads), compared to absence of Sox9 in the RP of control embryos. RFP was co-electroporated in both groups. Dashed lines delineate the RP domain. (J) Measurement of Sox9 staining intensity. For quantification, 15 sections per embryo were analyzed. Imaging and analysis were performed at somite levels 25-27. N = 10, 7, and 11 embryos for control, Cyp26A1 and RARα403 groups, respectively. *$p < 0.05$, ****$p < 0.0001$,

one-way ANOVA with post-hoc Tukey's tests. Abbreviations, NT, neural tube, DRG, dorsal root ganglion. Scale bar, 50 μm.

298 **RA signaling promotes cell cycle exit and epithelial traits in dorsal NT cells**

299 NC cells proliferate extensively while residing in the NT and also during migration. Upon the
300 end of NC production, dorsal NT progenitors gradually exit from the cell cycle to become post-
301 mitotic RP cells (Kahane and Kalcheim, 1998; Nitzan et al., 2016). We asked whether RA
302 inhibition affects cell cycle withdrawal of nascent RP cells. To this end, we immunostained
303 embryos at E4 (RP stage) for the mitotic marker phosphohistone H3 (pH3), following
304 electroporation of RARα403 or Cyp26A1 at E2.5 (NC stage). Remarkably, a significantly
305 higher number of mitotic nuclei was observed in the RP of embryos treated with either
306 Cyp26A1 or RARα403 compared to controls which exhibited a low extent of mitosis (Fig. 4A-
307 D). These results suggest that endogenous RA inhibits cell proliferation, consistent with
308 previous data obtained in forebrain and optic tectum of avian embryos (Gupta and Sen, 2015;
309 Kukreja et al., 2020).

310 Furthermore, characteristic of post-mitotic, differentiating progenitors is the localization of
311 nuclei to the basal domain of the neuroepithelium, as observed in control embryos at the RP
312 stage (Fig. 4E). In contrast, in RARα403-electroporated embryos, nuclei were spread
313 throughout its apico-basal extent. Quantification showed that their localization to the apical
314 half of the epithelium significantly exceeds that seen in control conditions (Fig. 4E-G). This is
315 consistent with the higher extent of cell proliferation monitored in the absence of local RA
316 signaling, reflecting the retention of interkinetic nuclear migration with presence of mitotic
317 nuclei in the ventricular zone, and/or a disorganization of the nascent RP under experimental
318 conditions.

319 Another critical process that occurs following the end of NC emigration is the restoration of
320 epithelial cell traits in the nascent RP (Nitzan et al., 2016). One of these traits is the deposition
321 of a continuous and prominent laminin-containing basal lamina covering the normal RP (Fig.

322 4H,H'). This basal lamina is incomplete at the NC stage due to continuous cell delamination.
323 Inhibition of RA signaling resulted in a weaker and discontinuous pattern of laminin
324 immunostaining dorsal to the RP (Fig. 4I-J), indicative of the maintenance of NC
325 characteristics at the later RP stage. Consistently, upon electroporation with membrane-
326 tethered GFP, it was apparent in controls that cells extended along the apico-basal domain of
327 the RP (Fig. 4H). In contrast, in the absence of RA activity, many cells were devoid of epithelial
328 integrity, including labeled cells detaching from the epithelium (Fig.4I, arrows). Combined,
329 these results show that inhibition of RA signaling in the dorsal NT prevents cells from exiting
330 the cell cycle and from adopting cellular traits that characterize the normal ontogeny of a RP.

331

332

Figure 4

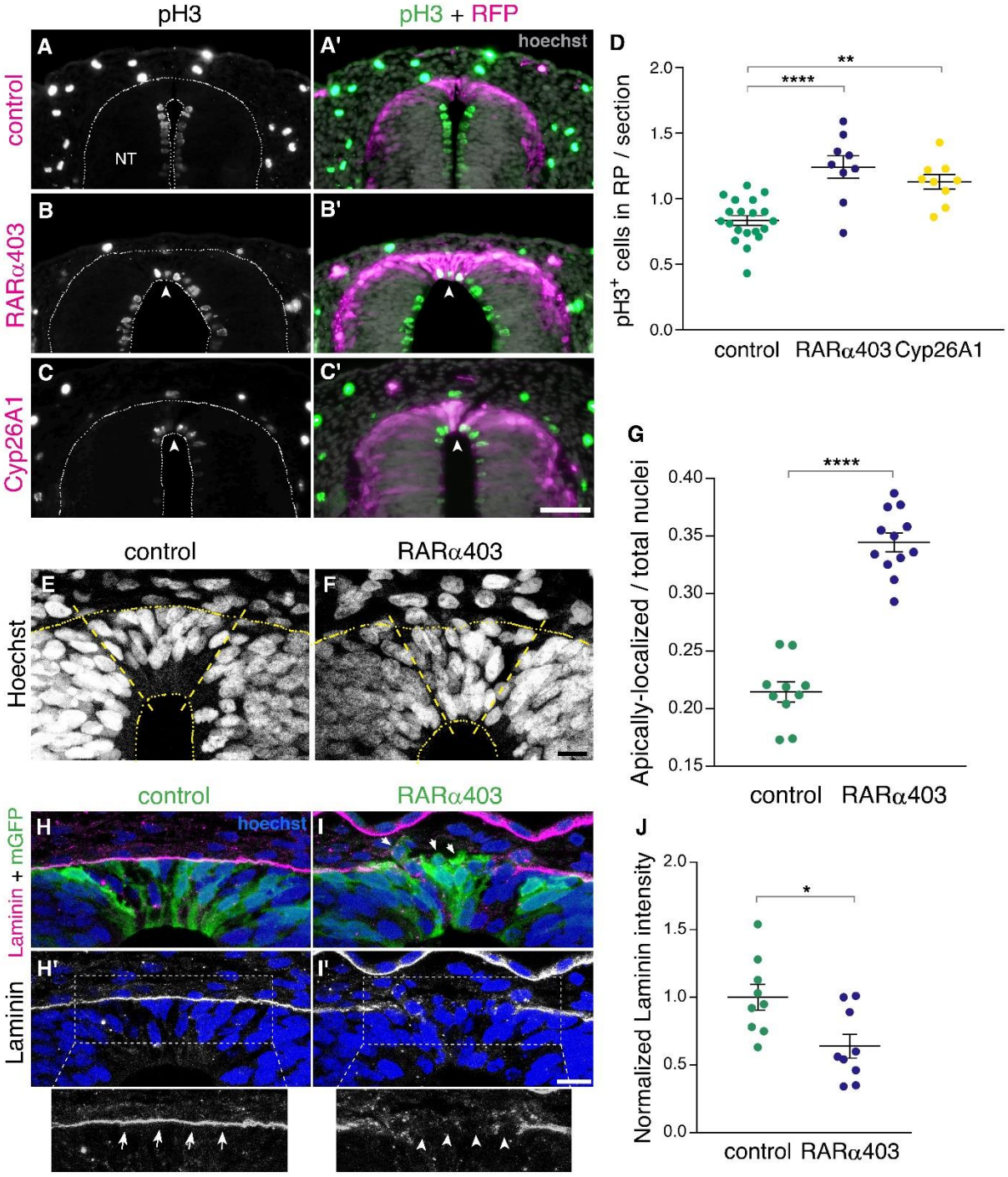

333

334 Figure 4- RA signaling promotes cell cycle exit and epithelial traits in dorsal NT cells

335 (A-D) Immunostaining for phospho-Histone H3 of embryos electroporated at E2.5 (27 ss) with either
336 control PCAGG, RARα403 or Cyp26A1, and analyzed at E4. Arrowheads in B-C' point to $pH3^+$ cells
337 in the RP domain of RARα403- and Cyp26A1-electroporated embryos. The quantification of $pH3^+$
338 cells in the RP is represented in (D). 120 sections were analyzed per embryo. Imaging and analysis were
339 performed at somite levels 24-26. N = 20, 9 and 9 embryos for control, RARα403 and Cyp26A1,
340 respectively. **$p < 0.005$, ****$p < 0.0001$, one-way ANOVA with post-hoc Tukey's tests.

341 (E-G) Apico-basal localization of Hoechst-stained nuclei in embryos electroporated as in A-D. Whereas
342 in control embryos most nuclei are restricted to the basal domain of the RP, in the RP of RARα403-
343 treated embryos, nuclei are apparent across the entire thickness of the tissue. Confocal images were z-
344 stacked and nuclei in the apical and basal halves of the RP domain were counted. The proportion of
345 apically-localized nuclei is represented in (G). Thirteen-to-17 sections were analyzed per embryo.
346 Imaging and analysis were performed at somite levels 25-27. N = 10 and 12 embryos for control and
347 RARα403 groups, respectively, ****$p < 0.0001$, exact p-value Mann-Whitney test.

348 (H-J) Immunostaining for Laminin of embryos electroporated as in A-D. Arrows and arrowheads in
349 insets of H' and I' indicate the presence of either a continuous or a discontinuous RP basal lamina,
350 respectively. Arrows in I point to delaminating cells. (J) Quantification of Laminin intensity along the
351 basal aspect of the RP. Six-to-18 sections were analyzed per embryo. Imaging and analysis were
352 performed at somite levels 25-27. N = 9 embryos both for control and RARα403 treatments. *$p <$
353 0.05, Student's unpaired t-test. Abbreviations, NT, neural tube. Scale bar, (A-C), 50 μm, (E-F, H-
354 I), 10 μm.

355 **RA is responsible for the end of NC delamination**

356 As described above, inhibiting RA activity in the dorsal NT extends the period of BMP activity
357 and preserves NC properties such as premigratory genes and cell proliferation into the RP stage.
358 We therefore asked whether the most discernible difference between NC cells and definitive
359 RP cells, the process of EMT and cell delamination, is prolonged as well by manipulation of
360 RA signaling.

361 To this end, we implemented a double electroporation protocol: first, we electroporated
362 RARα403 along with RFP only to one hemi-NT at E2 and at E3.5 both sides were labeled with
363 GFP-DNA (Fig. 5A). By E4, RFP-positive NC cells exited the NTs under both control and
364 treated conditions primarily towards the side ipsilateral to the transfection and also to some
365 extent towards the contralateral side, as previously described (Burstyn-Cohen and Kalcheim,
366 2002; George et al., 2007). However, the number of emigrated, late GFP-labeled cells was
367 significantly higher on the RARα403-electroporated side when compared to the control
368 contralateral side and also to both sides of control embryos (Fig. 5B-D, arrowheads in C').
369 These data show that RA signaling promotes the end of NC cell delamination.

370 Even though we observed that loss of RA activity stimulates sustained pSmad expression (Fig.
371 2B-D) and abrogates transcription of BMP inhibitors (Fig. 2F-O) along with extended NC
372 emigration (Fig. 5A-D), it is possible that this late EMT elicited by loss of RA is BMP-
373 independent. If that were true, then inhibition of BMP with Smad6 (Nitzan et al., 2016), should
374 be without effect on cell emigration induced by RARα403 at the RP stage.

375 To test this hypothesis, embryos aged E2 were bilaterally electroporated (Fig. 5A, bottom) with
376 either control GFP, RARα403 to induce late NC delamination (Fig. 5B-D), with Smad6, or
377 with both RARα403 and Smad6. At E3.5, control GFP was bilaterally delivered to all embryos
378 and the outcome was analyzed at E4 (Fig. 5A). In all cases, RFP-labeled cells that indicate the

379 efficiency of early transfections, successfully delaminated from the NT. In contrast, under
380 control conditions, few or no GFP-labeled cells delaminated from the NT (Fig.5E-E',I),
381 consistent with the second electroporation being done following the end of NC emigration. As
382 also shown above, in RARα403-treated embryos, a substantial number of GFP-labeled cells
383 had emigrated (Fig. 5F-F',I and see also D). As expected from late electroporations, treatment
384 with Smad6 alone resembled the control situation with few delaminated GFP^+ cells at the RP
385 stage (Figure 5G-G',I). Co-transfection of Smad6 and RARα403 inhibited the RARα403-
386 dependent extension of cellular EMT (Figure 5H-H',I). Together, these results suggest that late
387 RA signaling ends the period of cell emigration in a BMP-dependent manner.

388 Next, we examined whether the late-delaminating cells exhibit a NC identity. For this purpose,
389 embryos double-electroporated as described in Fig. 5A were immunostained for the NC marker
390 HNK1. While in control embryos no GFP-labeled cells were apparent outside the NT, and
391 HNK1 stained only NC derivatives such as dorsal ganglia and ventral roots, in RARα403-
392 treated embryos a considerable number of GFP^+HNK1^+ cells was also detected in the
393 mesenchyme near the NT (Fig.5 Supp.1A-B", arrowheads in B-B"). Remarkably, 95 ± 0.8%
394 of the late-delaminating GFP-labeled cells were $HNK1^+$ (Fig.5 Supp.1C), confirming their NC
395 nature.

396 In addition, we examined the pattern of *foxd3*, which is expressed both in premigratory and
397 migrating NC cells. Embryos were electroporated with RARα403 along with GFP at E2.5 and
398 analyzed at E4. Control NTs were devoid of *foxd3* mRNA in the RP and mRNA signal was
399 only detected in NC derivatives and dI2/V1 interneurons. In RARα403-treated embryos *foxd3*
400 expression was evident in the dorsal NT (see also Fig. 3), and also in NC cells that presumably
401 emigrated recently (Fig.5 Supp.1D-E', arrowheads), further confirming their NC identity.

402 Thus, local RA inhibition in the NT extends the period of NC production and further
403 delamination into the RP stage. Collectively, these results point to RA being a major regulator
404 of the end of the NC stage.

405 **Gain of RA signaling in the NT does not cause premature downregulation of BMP**
406 **signaling or end of NC EMT**

407 As precedently shown, the dorsal NT at the NC stage is characterized by the presence of BMP
408 activity, expression of various NC-specific genes and NC emigration (Figs.2,3,5). Likewise,
409 RA activity is also apparent in NT at this stage (Fig. 1N), suggesting that NC production and
410 emigration are compatible with the endogenous level of RA signaling observed. Since
411 repressing intrinsic RA activity prolongs NC-specific behaviors, we examined whether gain of
412 RA function beyond the normal level of activity could inhibit prematurely the occurrence of
413 NC traits. To this end, we electroporated a constitutively active form of human RAR-alpha
414 fused to the transcriptional activator domain of VP16 (VP16-RARα) that activates RA target
415 genes in a ligand-independent manner (Novitch et al., 2003). VP16-RARα significantly
416 enhanced RA signaling, as measured with a short-lived RARE reporter (Fig.5 Supp.2A-C).
417 Next, we monitored BMP activity (pSmad1/5/9), expression of Sox9 protein and *foxd3* mRNA
418 in embryos fixed at advanced stages of NC production prior to the normal downregulation of
419 the above. The number of sections or segments with pSmad, Sox9 or *foxd3* expression did not
420 differ between control and VP16-RARα–treated cases (Fig.5 Supp.2D-N, see details in
421 legend). Next, the extent of NC emigration was reduced by 19% (p=0.065, not significant) in
422 VP16-RARα compared to control GFP-transfected NTs. Although this could reflect a tendency
423 to a premature end of NC EMT, this limited effect could also be accounted for by death of
424 some VP16-RARα–transfected cells, frequently observed in the lumen of the experimental
425 cases, but not in controls (Fig.5 Supp.3). Together, whereas RA signaling is necessary for the

426 end of NC EMT and associated events, it is not sufficient to prematurely end these processes.
427 This could suggest that it is not the sole activity of RA in the NT that causes the end of NC
428 EMT but rather an interplay between RA signaling in the context of a gene network that
429 changes between NC and nascent RP stages.

430

431

Figure 5

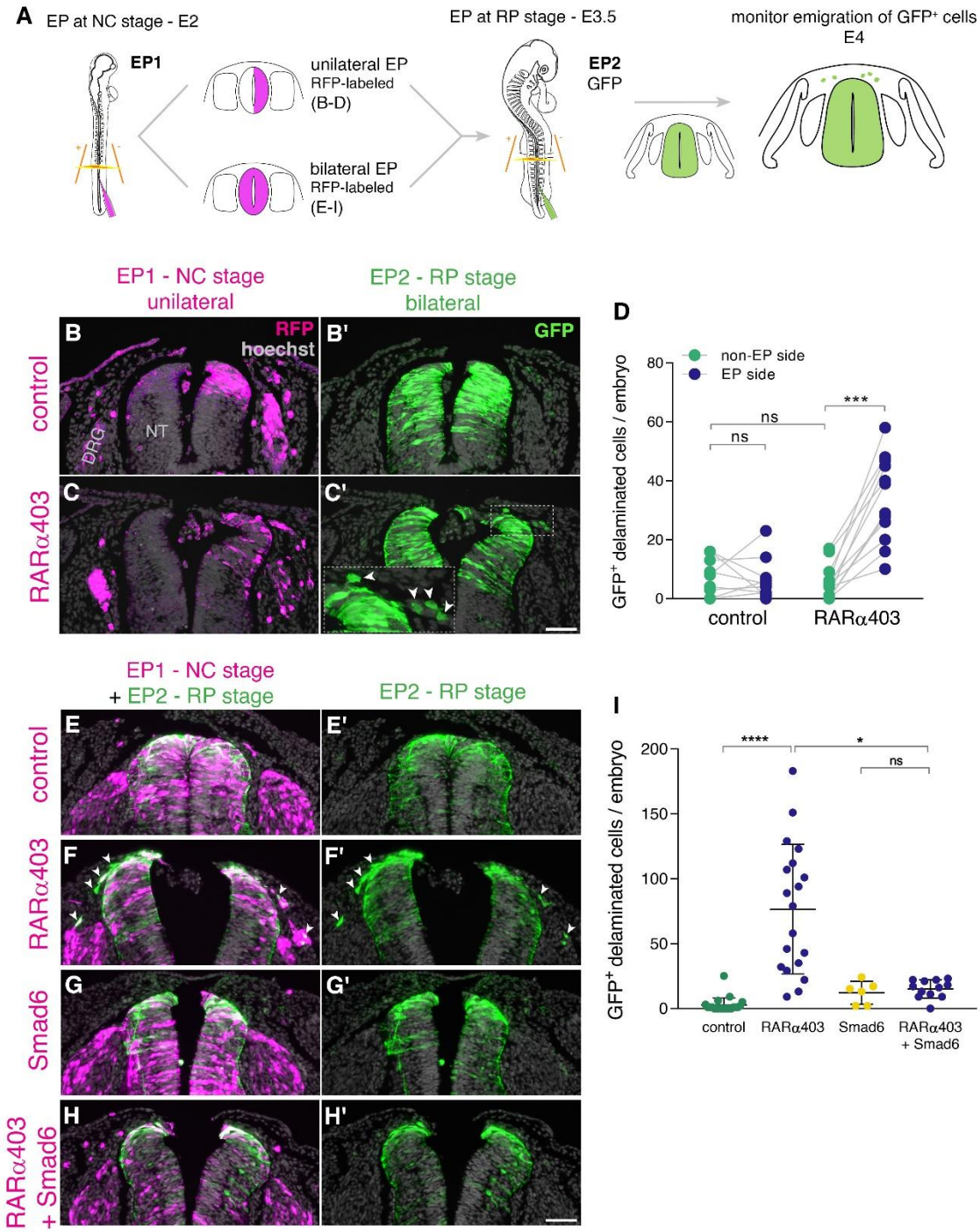

Figure 5 - RA is responsible for the end of NC delamination

(A) Schematic representation of the experimental design for detection of late-emigrating cells (see text for details). (B-D) Embryos electroporated unilaterally at E2 (22-23ss) with either control or RARα403 plasmids, followed by a second bilateral electroporation at E3.5 with control GFP. Emigration of GFP$^+$ cells was compared between electroporated and non-electroporated sides of control and experimental embryos at E4 (D). RFP was delivered with the early electroporation to monitor transfection efficiency. Images presented are adjacent to the rostral somitic domain. Whereas few GFP$^+$ cells delaminated at

440 the RP stage in controls, C' and inset show late-delaminating GFP^+ cells ipsilateral to the early
441 RARα403 electroporation (arrowheads). (D) Quantification of GFP^+ cells that emigrated from either
442 intact or electroporated (EP) sides of control and experimental embryos. Seventy two sections per
443 embryo were analyzed at somitic levels 23-25. N = 10 and 11 embryos for control and RARα403
444 groups, respectively. Statistical tests applied were exact P-value Wilcoxon signed ranks paired test to
445 compare between EP and non-EP sides of embryos inside each experimental group, and exact P-value
446 Mann-Whitney test to compare between non-EP sides of control and RARα403 groups. ***$p < 0.001$.

447 (E-I) Embryos were electroporated bilaterally at E2 (22-23ss) with control, RARα403, Smad6 or
448 RARα403+Smad6 constructs along with RFP. At E3.5, bilateral electroporations with GFP were
449 performed and embryos were analyzed for emigration of GFP^+ cells at E4. Images presented are
450 opposite a rostral somitic domain. Note the presence of emigrated RFP^+ cells in all treatments. Notice
451 as well the presence of GFP^+ delaminated cells in F,F', while virtually no GFP^+ cells are seen outside
452 of the NT in E,E', G,G' and H,H'. (I) Quantification of delaminated GFP^+ cells. Seventy sections per
453 embryo were analyzed at somite levels 23-25. N = 21, 19, 6 and 12 embryos were monitored for
454 control, RARα403, Smad6 and Smad6+RARα403 groups, respectively. *$p < 0.05$, ****$p < 0.0001$,
455 approximate P-value Kruskal-Wallis with post-hoc Dunn's test. Abbreviations, ns, not significant;
456 NT, neural tube, DRG, dorsal root ganglion. Scale bar, 50 μm.

457

458 **Inhibition of RA signaling downregulates only a subset of RP markers**

459 A major question that remains to be addressed is whether the end of the NC stage is sufficient
460 for signaling the formation of the definitive RP, or whether these are two independently
461 regulated processes. Given that RA deficiency delays the end of the NC stage, we asked
462 whether this occurs at the expense of timely RP development.

463 As recently shown (Ofek et al., 2021), there are differences in the gene expression profile
464 between premigratory NC cells and definitive RP cells. We selected a number of RP-specific
465 genes that are not expressed in the dorsal NT during the NC stage and examined the effect of
466 RA downregulation on their expression. As described in Fig. 2, expression of RP-specific BMP
467 inhibitors was strongly reduced. Likewise, mRNA encoding *Slit1*, a chemorepellent of post-
468 floor plate commissural axons (Kidd et al., 1999) was also decreased under experimental
469 conditions (Fig.6 Supp.1). In contrast, additional RP markers, such as *Rspo1, NDP (norrin)* or
470 *draxin*, were normally expressed (Fig.6 Supp.1), suggesting that development of a number of
471 RP traits is independent of RA signaling.

472 Since both NC and RP markers are present at the RP stage upon inhibition of RA signaling
473 (Fig.3, Fig.6 Supp.1), we proceeded to clarify whether NC and RP markers are expressed in
474 the same cells, or, alternatively, whether there is a mix of different cell types in the RP of
475 RARα403-treated embryos. First, we performed ISH of *Rspo1* (RP marker) and *foxd3* (NC
476 marker) on adjacent sections of RP-stage embryos electroporated at E2.5 with either RARα403
477 or control GFP (Fig. 6). Whereas in control NTs, only *Rspo1* was apparent in the RP, both
478 *Rspo1* and *foxd3* were detected in an overlapping pattern in the RP of the treated embryos (Fig.
479 6A-B'''').

480 In addition, we combined a fluorescent ISH of *Rspo1* with immunostaining for SNAI2 or Sox9
481 in the same sections. Control NTs exhibited SNAI2 and Sox9^{+} nuclei only outside the *Rspo1*$^{+}$

482 RP (Fig.6C-C'', E-E", see also Fig. 3). In striking contrast, both markers were detected in the
483 same dorsal NT cells in the absence of local RA signaling (Fig. 6D-D", F-G", H,I). In some
484 instances, *Rspo1*$^{+}$Sox9^{+} cells were also noticed undergoing delamination from the NT (Fig.
485 6G-G", arrowhead).

486 Next, we examined whether gain of RA function implemented at the NC stage, is able to cause
487 a premature onset of expression of selected RP genes. Serial section analysis, performed in
488 regions flanking the beginning of gene expression, revealed that the onset of both *BAMBI* and
489 *Rspo1* mRNAs in the NT was similar in control and VP16-RARα-treated embryos (Fig.6
490 Supp.2).

491 Together, these data show that the loss of RA signaling does not totally prevent the advent of
492 RP markers and, reciprocally, high levels of RA signaling at the NC stage are not sufficient to
493 promote a premature advent of RP-specific genes. Hence, loss of NC identity and gain of RP
494 fate are independently-regulated processes. Nevertheless, timely RA activity in the dorsal NT
495 is required for the proper segregation of NC from RP fates.

496

497

Figure 6

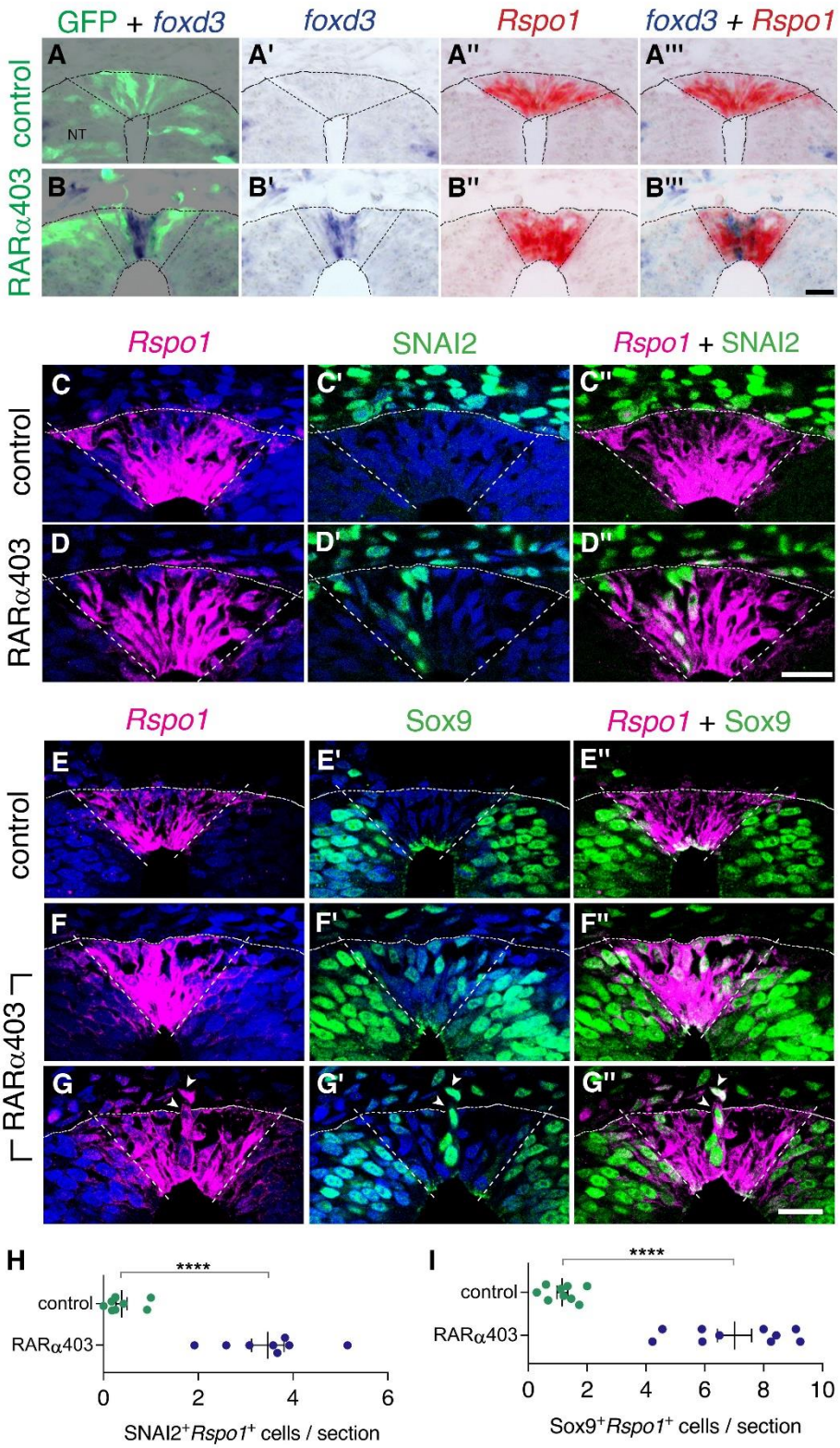

Figure 6 - Overlapping expression in RP of both NC and RP markers upon inhibition of RA signaling

(A-B'''') Embryos co-electroporated at E2.5 (27ss) with either control PCAGG or RARα403 along with a GFP plasmid. Embryos were fixed at E4, and adjacent sections were in-situ hybridized for *foxd3* or *Rspo1* and then superimposed to reveal overlapping domains of gene expression. Dotted lines delineate

503 the *Rspo1* expression domain. In control embryos, no *foxd3* expression was detected in the RP (N = 2,
504 and see also Fig. 3). In RARα403-treated embryos, overlapping expression was detected in all 4
505 embryos examined. Imaging and analysis were performed somite levels 24-26.

506 (C-D") Immunostaining for SNAI2 and fluorescent ISH for *Rspo1* were combined on the same
507 sections of embryos electroporated at E2.5 (27ss) with either control PCAGG or RARα403 and
508 analyzed at E4. Dashed lines mark the *Rspo1* expression domain. Note the presence of SNAI2^{+}*Rspo1*$^{+}$
509 cells in the RP in D". (E-G") Immunostaining for Sox9 and fluorescent ISH for *Rspo1* were
510 performed as above. Note the presence of Sox9^{+}*Rspo1*$^{+}$ cells in the RP in F" and G''. Additionally,
511 delaminating Sox9^{+}*Rspo1*$^{+}$ cells (arrowheads in G-G") were apparent under experimental conditions.
512 (H,I) Quantification of SNAI2^{+}*Rspo1*$^{+}$ and Sox9^{+}*Rspo1*$^{+}$ cells in the RP. Imaging and analysis were
513 performed at somite levels 24-26. N = 8 and 8 for SNAI2 in controls and RARα403. N = 9 and 10
514 embryos for control and RARα403 groups stained with Sox9, respectively. ****$p < 0.0001$, Welch's
515 t-test. Abbreviations, NT, neural tube. Scale bar, 20 μm.

516

517 **RP-derived dI1 interneuron development only partly depends on RA signaling**

518 We further investigated whether depletion of RA signaling had any effect on the role of the RP
519 as a signaling center for dorsal interneuron development. We immunostained RARα403 and
520 control-electroporated embryos with the dI1 interneuron marker BarHL1, and analyzed the
521 number of BarHL1$^+$ cells and their spatial distribution. Whereas no significant difference in
522 the number of BarHL1$^+$ interneurons could be monitored between control and treated embryos
523 (Fig. 7A), there was a collective dorsal shift in their position in the RARα403-treated NTs,
524 with some of BarHL1$^+$ cells residing in the RP domain itself (Fig. 7B-E', arrowheads). This
525 shift did not impact the overall size of the RP, as the area of the *Rspo1*-positive RP did not
526 significantly differ between control and treated embryos (control, 1672 ± 121.3 μm^2 (n = 8);
527 compared to RARa403, 1790 ± 146.1 μm^2 (n=8), p = 0.544, student's t-test).

528 Thus, whereas inhibition of RA signaling does not affect RP-mediated formation of dI1
529 interneurons, it interferes with the spatial information conveyed onto dorsal interneurons from
530 the RP, likely by impairing the formation of the boundary between the RP and more ventral
531 domains. These findings further indicate that RA signaling not necessarily influences
532 development of RP properties but rather impairs temporal and spatial segregation between
533 dorsal cell lineages.

534 Data from young caudal neural plate explants and from VAD embryos that lack RA, showed
535 that early RA signaling from developing somites is required for dorso-ventral patterning of the
536 NT, for the specification of ventral cell types (motoneurons and V1, V2 interneurons) and for
537 neuronal differentiation (Del Corral et al., 2003; Liu et al., 2001; Sockanathan and Jessell,
538 1998; Wilson et al., 2004). We therefore examined whether later inhibition of RA activity as
539 performed in the present context merely concerns the dorsal NT or, alternatively, has a general
540 effect on dorso-ventral patterning. To this end, we examined the effects of bilateral RA

541 attenuation on the expression of Pax7 in the dorsal NT, and of the motoneuron-specific protein
542 Hb9. RARα403 caused a mild 12% increase in the area of expression of Pax7 when compared
543 to controls (Fig.7 Supp.1A-C), and had no effect on either the localization or extent of
544 expression of Hb9 (Fig.7 Supp.1D-F). These data corroborate that the effects documented are
545 directed to the dorsal NT and do not result from overall changes in its dorso-ventral patterning.

546

Figure 7

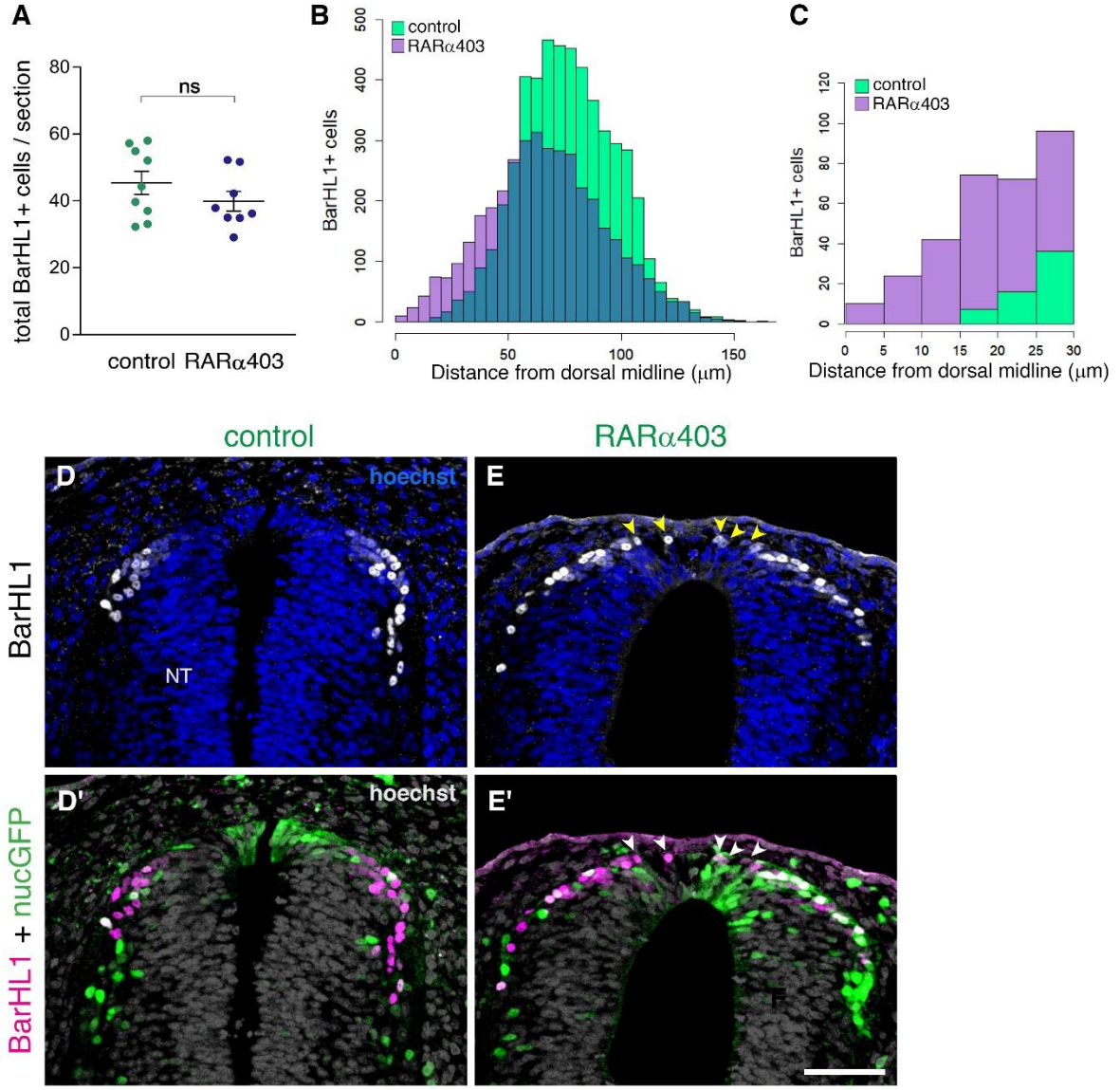

547

548 Figure 7- RP-derived dI1 interneuron development only partly depends on RA signaling

549 (A) Quantification of BarHL1^{+} dI1 interneurons in E4 embryos, electroporated at E2.5 (27ss) with either
550 control PCAGG or RARα403. No significant difference in the number of BarHL1^{+} neurons was
551 monitored. Ten-to-14 sections were analyzed per embryo; N= 9 and 8 embryos for control and
552 RARα403 groups, respectively. Student's unpaired t-test was applied.

553 (B, C) Spatial distribution of BarHL1^{+} cells measured as the distance from the dorsal midline. 5126
554 cells were counted in the control group (green), and 3886 in the RARα403 group (purple). The area of
555 overlap of control and experimental cells is in blue. Note the dorsal shift of cells in the RARα403-
556 treated group when compared to controls. In (B) all the cells are included, while in (C) only cells
557 included in a 30 μm distance from the dorsal midline, comprising the RP region, are presented.

558 (D-E') Confocal images of BarHL1-stained sections. Nuclear GFP (nucGFP) marks the electroporated
559 domain. Note in E and E' the presence of BarHL1^{+} interneurons inside the RP domain (arrowheads)
560 compared to controls in which these neurons are localized ventral to the RP. Nuclei are visualized with
561 Hoechst. Abbreviation, NT, neural tube. Scale bar, 50 μm.

562 **The dorsal NT as the source of RA responsible for NC to RP transition**

563 As shown in Figs. 1 and Supp.1, the dorsal NT becomes a source of RA during the period
564 marking the end of NC emigration and transition to the RP stage, suggesting this is the local
565 source of RA that underlies the effects demonstrated here. Yet, at the same time, RA is still
566 produced in the adjacent paraxial mesoderm. To begin addressing whether the latter tissue
567 accounts for the effects observed, we separated the paraxial mesoderm from the NT with an
568 impermeable membrane and assessed the development of the RP. A unilateral slit was
569 performed at the epithelial somite stage into which a piece of aluminum foil was inserted (Fig.
570 8A). We analyzed RP formation using *BAMBI* expression as a sensitive readout for normal RP
571 ontogeny that is downregulated in the absence of RA signaling (Fig.2). Notably, *BAMBI*
572 remained strongly expressed in the RP of treated embryos to the same extent as the control
573 sides, despite separation from the mesoderm and virtual disappearance of the somitic tissue
574 that lost contact with the NT (Fig. 8A-C'). To exclude the possibility that RA from the
575 mesoderm of the non-separated side is sufficient to induce normal RP development, a slit was
576 made along the dorsal midline of the NT following insertion of the barrier, thus opening the
577 NT and creating a physical gap between both halves of the neuroepithelium (Fig. 8D). A
578 comparable expression of *BAMBI* mRNA on both hemi-RPs was still apparent under these
579 conditions (Fig. 8E-F"), suggesting that the paraxial mesoderm is not the source of RA
580 important for NC to RP transition.

581 Next, we asked what restricts expression of *Raldh2* to the RP. *Foxd3, snai2* and *sox9* are
582 transcribed only during the NC stage in a complementary pattern vis-a-vis *Raldh2* (Krispin et
583 al., 2010b; Ofek et al., 2021). In addition, RP-derived RA inhibits expression of these three
584 transcription factors (Fig. 3). We therefore predicted that the onset of *Raldh2* production in RP
585 could be initiated by the normal downregulation of these NC-specific genes. To test this notion,
586 we extended the activity period of *foxd3, snai2* or *sox9* by misexpressing each of them close to

587 their time of disappearance from the dorsal NT (30ss at the flank level)(Krispin et al., 2010b)
588 and monitored *Raldh2* mRNA at the RP stage (E4). Each of the factors cell-autonomously
589 prevented the onset of *Raldh2* expression in the RP when compared to control GFP-
590 electroporated cases (Fig. 9). Hence, expression of NC (*foxd3, snai2, sox9*) and RA-associated
591 RP traits (e.g; *Raldh2*) stand in a mutually repressive temporal relationship. Together, these
592 interactions provide novel insights into the existence of a gene regulatory network responsible
593 for the transition between NC and RP (Fig.10).

594

Figure 8

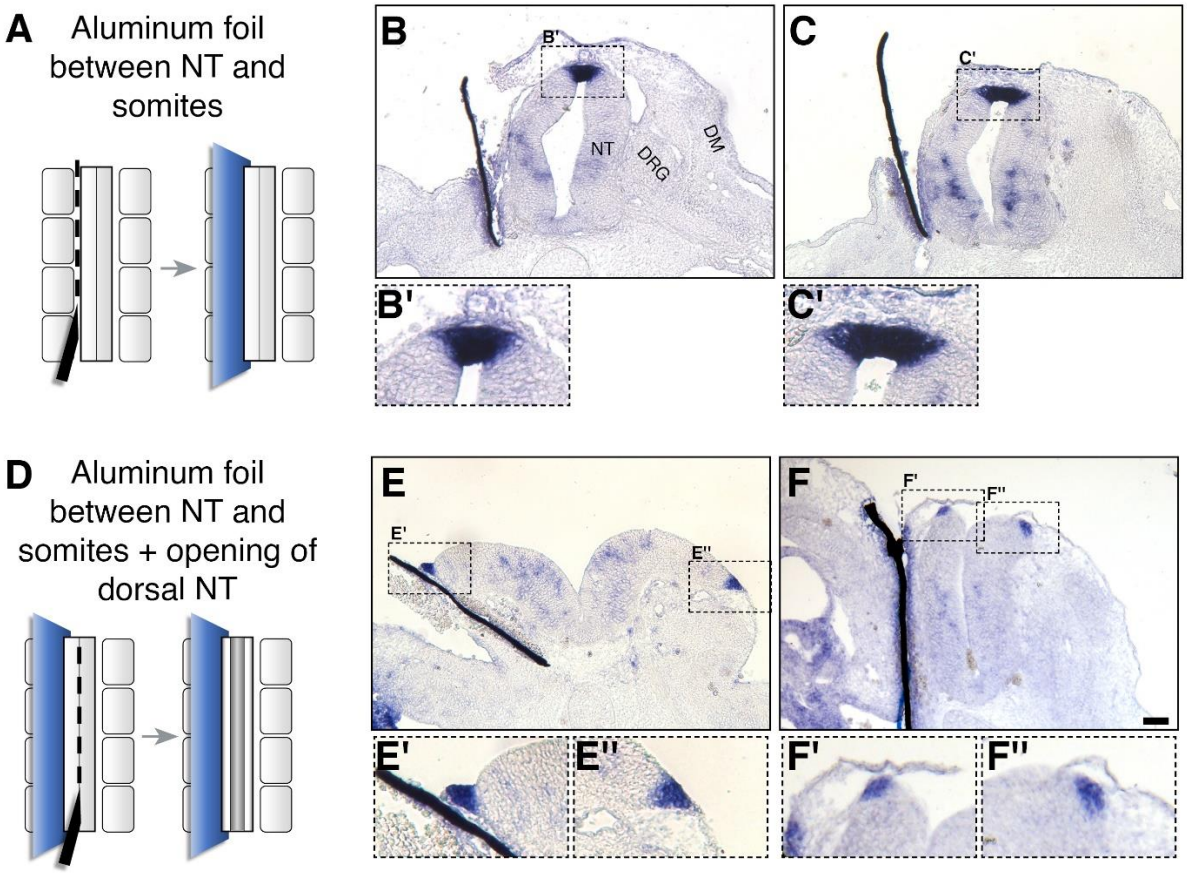

Figure 8- Somitic RA is dispensable for NC-to-RP transition

(A, D) Schematic representations of the experimental design to mechanically separate the NT from somitic mesoderm using an impermeable aluminum foil inserted at 27ss at the level of the rostral segmental plate and 5 newly formed somites. Embryos were fixed at E4.

(B-C', E-F') ISH for *BAMBI* on sections of embryos with intact (B-C') or split (E-F") dorsal NTs following grafting of a unilateral barrier between NT and somites. Representative images from two different embryos are presented for each treatment. *BAMBI* expression remained unchanged in the RP opposite to the operated sides in 7/7 embryos with an intact RP, and in 4/4 embryos with a split RP. Note as well that distal to the barriers, most of the somitic mesoderm disappeared (B,C,E). In some instances, the somatic layer of the lateral plate mesoderm approached the barrier (F). Abbreviations, DM, dermomyotome, DRG, dorsal root ganglion, NT, neural tube. Scale bar, 50 μm.

Figure 9

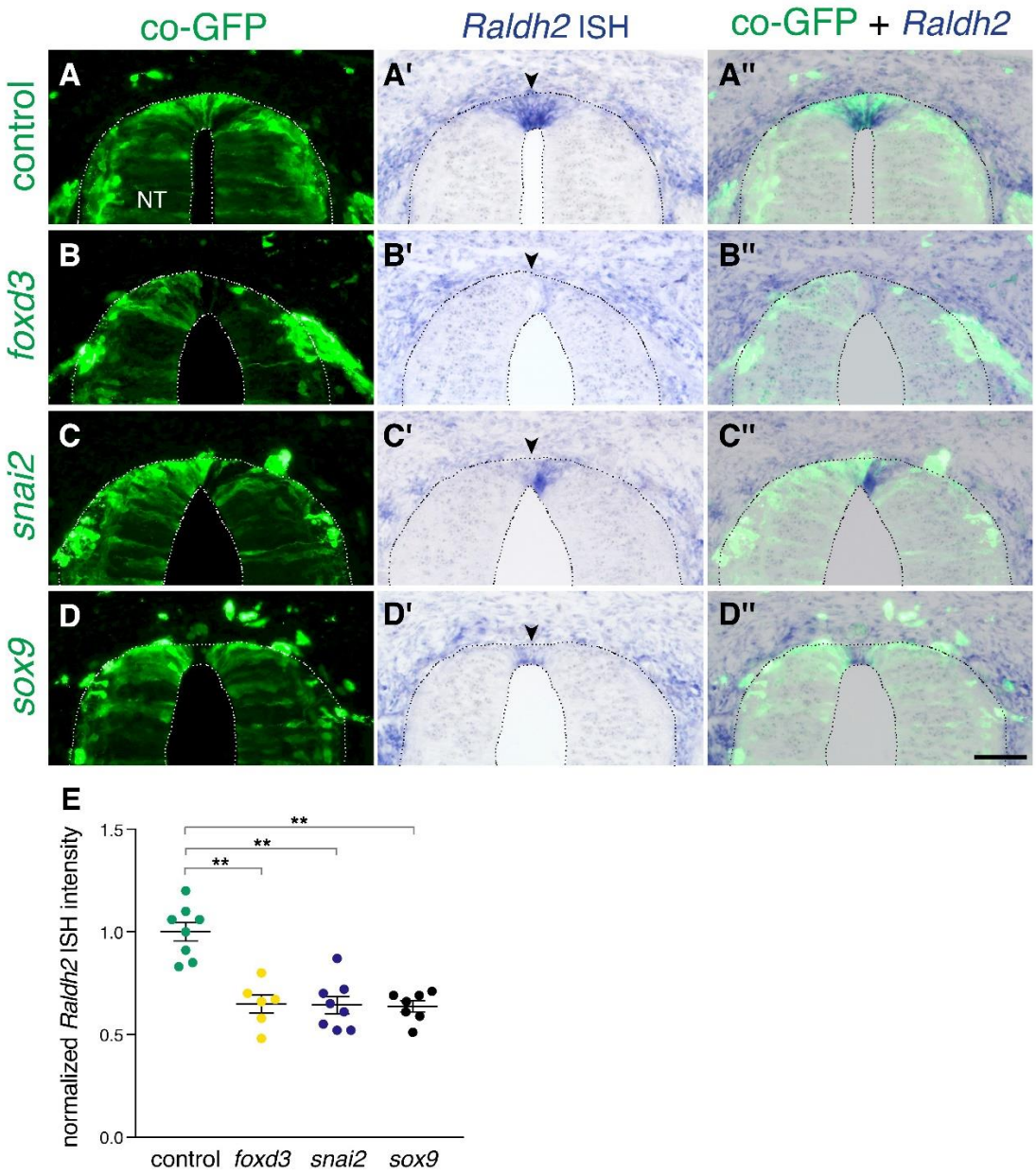

610

611 Figure 9 – Extension of the activity of NC-specific genes prevents the onset of expression of *Raldh2* in
612 the nascent RP

613 (A-D") Embryos were electroporated at E2.5 (27ss) with control unlabeled PCAGG vector or with
614 *foxd3*, *snai2* or *sox9*-expressing constructs along with GFP, and analyzed at E4 for expression of
615 *Raldh2*. Note the lack of *Raldh2* expression in the transfected cells of all treated groups compared to
616 controls (arrowheads).

617 (E) Quantification of *Raldh2* ISH intensity. 6-30 sections were analyzed at somite levels 24-26. N =
618 8,6,8 and 7 embryos for control, *foxd3*, *snai2* and *sox9* groups, respectively. **$p < 0.01$ via Kruskal-
619 Wallis with post-hoc Dunn's test. Abbreviations, NT, neural tube. Scale bar, 50 µm.

Figure 10

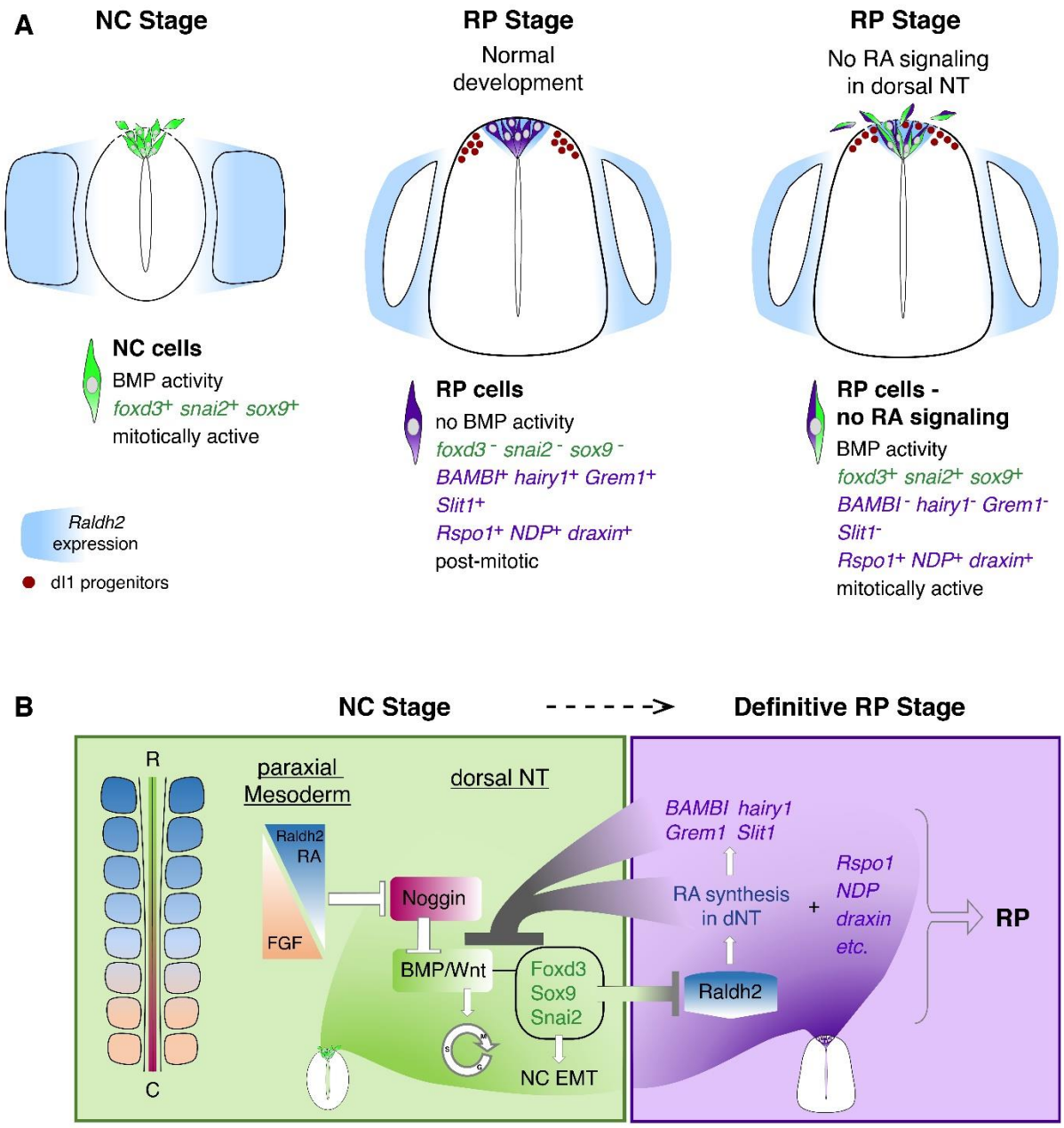

Figure 10- Schematic diagram summarizing the role of RA in the transition from NC to RP

(A, left panel) At the NC stage, premigratory progenitors residing in the dorsal NT (green) exhibit BMP signaling activity, express specific NC markers (e.g. *foxd3*, *snai2* and *sox9*, green) and proliferate extensively. Following a process of EMT, NC cells delaminate from the NT through a discontinuous basement membrane (dashed line) to migrate away. At the NC stage, RA is supplied to the NT from the paraxial mesoderm, where it is produced by Raldh2 (blue).

(A, middle panel) Under normal conditions, upon cessation of NC production and emigration, a definitive RP forms. RP cells (purple) are refractory to BMP signaling, and exhibit a different gene expression profile when compared to NC cells: they downregulate *foxd3*, *snai2* and *sox9* and upregulate

630 RP-specific genes (purple), among which are known inhibitors of BMP signaling. RP cells gradually
631 exit the cell cycle and do not delaminate, regenerating a continuous basement membrane and epithelial
632 traits. During the transition between NC and RP stages, *Raldh2* expression begins in the dorsal NT (blue
633 in RP), in addition to RA still produced in somites. The RP functions as a signaling center, regulating
634 specification and/or differentiation of dorsal interneurons (red, dI1 progenitors) that localize ventral to
635 the RP.

636 (A, right panel) In the present study we demonstrate that inhibition of RA signaling in the dorsal NT,
637 impairs the end of NC production and consequently, the normal transition between NC and RP stages.
638 First, under experimental conditions, dorsal NT cells at the RP stage retain active BMP signaling likely
639 via downregulation of BMP antagonists (*BAMBI, hairy1, Grem1*) otherwise selectively expressed in
640 RP. Second, they express both NC and RP markers (illustrated as green/purple cells), Third, they
641 functionally behave as NC cells, maintaining mitotic activity, impaired epithelial traits (such as a
642 discontinuous basement membrane, dashed line), and continuous emigration from the NT. Fourth,
643 although the advent of several RP-specific markers is normal (e.g; *Rspo1, NDP, draxin*) and the number
644 of dI1 progenitors (red circles) is unchanged, the spatial segregation between NC, RP and dI1
645 interneuron lineages is compromised.

646 (B) A proposed model for the transition between NC (green) and RP (purple) stages. At early stages,
647 reciprocal gradients of RA and FGF in the paraxial mesoderm result in downregulation of the BMP
648 inhibitor Noggin in the dorsal NT. This allows for the activation of BMP and Wnt signaling pathways,
649 which promote cell proliferation and induce NC EMT. As NC cells delaminate and leave the NT, NC-
650 specific genes (*foxd3, sox9* and *snai2*) are downregulated. Since the latter genes inhibit the synthesis
651 of *Raldh2* in the nascent RP, their disappearance enables the onset of *Raldh2* expression allowing for
652 the local synthesis of RA in RP. RA in turn inhibits BMP and consequently, Wnt signaling, either
653 directly or via upregulation of BMP inhibitors (*BAMBI, hairy1, Grem1*). We propose the existence of
654 mutual cross-inhibitory interactions between RA-responsive genes that characterize NC and RP
655 stages, respectively, in the temporal sequence leading to the formation of the definitive RP and its
656 segregation from NC.

657 **Discussion**

658 Here we show that dorsal NT-derived RA controls the end of NC production and emigration
659 (Fig.10). This effect is mediated through BMP signaling, at least via the upregulation of BMP
660 inhibitors in the nascent RP, which prevents persistent BMP activity and ensures the timely
661 cessation of NC production (Fig.10)(Nitzan et al., 2016). We previously reported that BMP
662 produced in the dorsal NT is an essential inducer of NC EMT and emigration; a graded activity
663 of BMP is created along the rostro-caudal axis of the embryo thanks to a counter-gradient of
664 its inhibitor noggin. By the time of initial somite dissociation, noggin expression is
665 downregulated by somite derived factors (Sela-Donenfeld and Kalcheim, 1999; Sela-
666 Donenfeld and Kalcheim, 2002), later found to be accounted for by an interplay between
667 mesodermal RA and Fgf8 (Martínez-Morales et al., 2011). This group reported that during
668 gastrulation, RA is required for NC specification, as revealed by analysis of VAD quail
669 embryos. Next, during somite formation, somite-derived RA is necessary for the onset of
670 emigration of specified NC progenitors but at advanced somite stages it is dispensable for the
671 subsequent maintenance of cellular EMT (Martínez-Morales et al., 2011). Together, these and
672 the present results highlight a rather complex behavior of RA at four sequential stages of NC
673 ontogeny, specification, onset, maintenance and completion of EMT.

674 Our findings are consistent with previous results reporting that RA repressed BMP signal in
675 P19 embryonic carcinoma cells; in vivo, RA antagonized BMP-regulated differentiation and
676 proliferation of neural progenitor cells in the NT (Sheng et al., 2010). Likewise, RA was also
677 found to inhibit Wnt signaling (Shaker et al., 2020), that in the present context acts downstream
678 of BMP and whose activity was extended in RP by loss of RA signaling.

679 In normal development, the end of NC emigration is followed by the advent of the definitive
680 RP of the CNS (Rekler and Kalcheim, 2021). This is associated with a progressive withdrawal

681 from the cell cycle, the regeneration of a complete basal lamina overlying the dorsal NT, of
682 apico-basal properties of the RP epithelium and the corresponding downregulation and
683 upregulation, respectively, of NC and RP-specific genes (Nitzan et al., 2016; Ofek et al., 2021).
684 We report that, in the absence of RA activity, there is a continuity of several molecular and
685 cellular properties of the NC well into the RP stage, including the presence of a subset of RP
686 cells that co-expresses NC markers. Together, lack of local RA activity blurs the spatial and
687 temporal segregation between NC and RP (Fig. 10A).

688 Despite these phenotypes, it is notable that RP-specific markers such as *Rspo1*, *NDP* or *draxin*,
689 were not affected, suggesting that a RP is able to develop even if RA activity is inhibited. This
690 raises the fundamental question whether the end of NC formation and the ensuing development
691 of a RP are regulated by the same or by independent mechanisms. Our results would suggest
692 that the mechanisms accounting for the cessation of NC phase are necessary but not sufficient
693 to explain all aspects of RP development. Consistent with this notion, spatio-temporal lineage
694 tracings revealed that RP segregate from neural progenitors of the NC before the latter
695 complete emigration (Krispin et al., 2010b; Nitzan et al., 2012). In addition, gain and loss of
696 Notch function in avians and mice, respectively, resulted in changes in RP formation with no
697 apparent effects on NC cell behavior (Ofek et al., 2021). This would indicate that although NC
698 and RP lineages arise from common progenitors (Bronner-Fraser and Fraser, 1988; Nitzan et
699 al., 2012) by different exposure times and/or levels of BMP signaling (Nitzan et al., 2016;
700 Timmer et al., 2002; Tozer et al., 2013), they segregate rather early from each other.

701 Among the RP genes whose expression is perturbed in the absence of RA signaling, we found
702 *BAMBI, HES/hairy1* and *Grem1*, none of which is expressed in the dorsal NT at NC stages.
703 These genes, whose transcription was prevented by treatment with RARα403 and/or Cyp26,
704 encode inhibitors of BMP signaling. Furthermore, HES represses BMP activity and subsequent
705 NC emigration (Nitzan et al., 2016). Hence, RA-sensitive aspects of RP development are linked

706 to its regulation of BMP activity. Moreover, since RA-dependent downregulation of BMP
707 activity accounts for only selected facets of RP ontogeny, we posit that RP development
708 comprises both RA-dependent and RA-independent mechanisms.

709 We observed that maintenance of NC traits in RARα403-treated NTs did not interfere with
710 differentiation of a normal number of RP-dependent dorsal interneurons of type 1, suggesting
711 that the role of the RP as an interneuron inducer center was not altered. However, their
712 topographical dorsoventral distribution was abnormal as instead of organizing into discrete
713 nuclei, interneurons redistributed along the basal surface of the NT comprising the RP itself,
714 further demonstrating that the structural integrity of this signaling center and/or of its
715 boundaries is compromised. This is consistent with the observed local changes in epithelial
716 architecture, cell cycle properties and basal lamina deposition and might be partially accounted
717 for by the continued emigration of NC cells driving a dorsal shift of interneurons. Along this
718 line, cell shape changes associated with continuous mitosis were reported to impact tissue
719 architecture, including epithelial polarity and cellular EMT (Despin-Guitard and Migeotte,
720 2021).

721 In addition, since dI1 interneurons are also specified by BMP signaling (Chesnutt et al., 2004;
722 Hegarty et al., 2013; Timmer et al., 2002), it is conceivable to speculate that maintenance of
723 BMP responsiveness in the RP of RARα403-treated NTs affects the normal dorso-ventral
724 gradient of BMP activity (Tozer et al., 2013), perhaps eliciting indirectly an attractive function
725 that enables dI1 interneurons to migrate into the RP domain. In this context, RP-derived BMP
726 exhibits at a later stage chemorepellent properties vis-à-vis commissural axons (Augsburger et
727 al., 1999; Butler and Dodd, 2003), putting forward the additional possibility of guidance
728 functions for this morphogen under the present experimental conditions. One of the genes
729 downregulated upon abrogation of RA function is *Slit1*, a known repellent of axonal guidance

730 (Kidd et al., 1999), as well as of cell migration (Halperin-Barlev and Kalcheim, 2011;
731 Theveneau and Mayor, 2012b). This is consistent with recent data pointing to an indirect role
732 for RA in axonal guidance (Isabella et al., 2020). Loss of *Slit1* in the absence of RA activity
733 could also account for the dorsal shift of dI1 interneurons into the RP domain, and possible
734 interactions between the three factors in this context remain to be explored.

735 As discussed precedently, the NT is sensitive to RA throughout development, with RA playing
736 various functions at different stages [this study, (Diez del Corral and Morales, 2014; Martinez-
737 Morales et al., 2011; Wilson et al., 2004)]. Hence, it is plausible that the mechanisms mediating
738 these effects differ as a function of time and context. Here we report that precisely before the
739 end of NC delamination, RA begins to be synthesized in the dorsal NT (e.g; *Raldh2* expression)
740 in addition to the paraxial mesoderm, raising the notion that this new, local source of RA
741 accounts for the end of NC development. Notably, *Raldh2* is also synthesized in the RP of
742 mouse embryos (Ofek et al., 2021). Unfortunately, available mutants of *Raldh2* are embryonic
743 lethal at about E8.75 (Niederreither et al., 1999), precluding a focal analysis of the transition
744 from NC to RP. In this sense, the avian embryo provides an excellent model to address events
745 restricted both in time and space. The first is the activity of somite vs. RP-derived RA. Two
746 methods we implemented to abrogate RA signaling in the dorsal NT that act primarily in a cell
747 autonomous fashion. However, it is still possible that given the secreted nature of the ligand,
748 Cyp26A1 and/or RARα403 misexpression in the dorsal NT also provide a sink for somitic RA.
749 Despite robust separation of the mesoderm from the NT, expression of *BAMBI*, a most sensitive
750 and significant readout of RA activity, was not altered, suggesting that mesodermal RA is
751 dispensable. What accounts for this shift in responsiveness from a mesodermal towards a neural
752 source of factor? First, local RA could provide a more efficient signal to target progenitors
753 given the increasing size of the embryo and the development of a continuous basement
754 membrane dorsal to the NT. Second, cofactors of RA such as *CRABP1*, could change the nature

755 of the cellular response as it only appears at the RP stage. Together, changes in the molecular
756 landscape between NC and RP stages (Ofek et al., 2021), that partly depend on local RA
757 activity, may alter the nature of the interactions between RA and BMP/Wnt to signal a timely
758 cessation of NC production.

759 Second, we asked what restricts the synthesis of *Raldh2* to the dorsal NT at the RP stage.
760 Whereas RP-derived RA inhibits NC-specific traits including transcription of *foxd3, sox9* and
761 *snai2*, each of these factors in turn represses the onset of *Raldh2* transcription in the nascent
762 RP. Thus, as long as NC genes are expressed in the early dorsal NT (NC stage), local *Raldh2*
763 and consequent RA synthesis does not take place. Hence, a cross-repressive interaction exists
764 between NC and RP-specific genes downstream of RA, an emerging temporal property of the
765 network that determines the segregation of sequential cell lineages (Fig. 10B).

766 Our study thoroughly documents a role of local RA activity on the end of NC production and
767 ensuing RP architecture. A comprehensive elucidation of the molecular mechanism/s
768 responsible for inhibition of BMP signaling by local RA is the next obligatory step. In this
769 regard, different RA enhancers might be expressed at either stage and be regulated by separate
770 factors. For example, a specific enhancer driving expression of *Raldh2* is activated only at the
771 definitive RP stage (Castillo et al., 2010). This enhancer contains Tcf binding sites and thus
772 may be activated by Wnt signaling. In turn, RP-derived Raldh2 and resulting RA could
773 negatively feedback on Wnt signaling in the formed RP either directly or through BMP acting
774 upstream of Wnt (Fig. 10B). Consistent with this possibility, we presently report that RP-
775 derived RA signaling induces expression of the BMP inhibitors *BAMBI, Grem1* and *hairy/hes*
776 specifically in RP, and this can be one mechanism whereby RA represses BMP signaling.
777 Along this line, we previously showed that misexpression of *Hes1* at the NC stage
778 downregulates BMP activity and represses NC EMT (Nitzan et al., 2016). Furthermore, RA

779 could repress BMP signaling by inactivating Smad proteins via ubiquitination, as shown to be
780 the case in selected cell lines (Sheng et al., 2010). Altogether, the present study provides an
781 initial mechanistic explanation for the completion of NC production and separation between
782 PNS (NC) and CNS (RP and dI1) lineages during development.

783

784 **Materials and Methods**

Key Resources Table				
Reagent type (species) or resource	**Designation**	**Source or reference**	**Identifiers**	**Additional information**
strain, strain background (Japanese quail)	*Coturnix coturnix japonica*	Moshav Mata	NCBI taxon: 93934	
antibody	anti-GFP (Rabbit polyclonal)	Invitrogen, Thermo-Fisher Scientific	Cat#A6455; RRID:AB_221570	IF(1:1000)
antibody	anti-GFP (Mouse monoclonal)	Abcam	Cat#Ab38689; RRID:AB_732715	IF(1:100) Not available anymore
antibody	anti-RFP (Rabbit polyclonal)	Acris	Cat# AP09229PU-N; RRID:AB_2035909	IF(1:1000)
antibody	anti-pSmad1/5/8 (guinea pig polyclonal)	E. Laufer	N/A	IF(1:300)
antibody	anti-pSmad1/5/9 (Rabbit monoclonal)	Cell Signaling Technology	Cat#CST13820; RRID:AB_2493181	IF(1:500)
antibody	anti-H3-pS10 (Mouse monoclonal)	Abcam	Cat#Ab14955; RRID:AB_443110	IF(1:400)
antibody	anti-Laminin (Rabbit polyclonal)	Sigma Israel	Cat#L9393; RRID:AB_477163	IF(1:100)
antibody	anti-Sox9 (Rabbit polyclonal)	Millipore	Cat#AB5535; RRID:AB_2239761	IF(1:150)
antibody	anti-SNAI2 (Rabbit monoclonal)	Cell Signaling Technology	Cat#CST9585; RRID:AB_2239535	IF(1:500)
antibody	anti-CD57(HNK1) (Mouse monoclonal)	BD Biosciences	Cat#559048; RRID:AB_397184	IF(1:500)

antibody	anti-BarHL1 (Rabbit polyclonal)	Sigma Israel	Cat# HPA004809; RRID:AB_1078266	IF(1:300)
antibody	anti-Pax7 (Mouse monoclonal)	DHSB	Cat# pax7; RRID:AB_528428	IF(1:10)
antibody	anti-Hb9 (mouse monoclonal)	DHSB	Cat# 81.5C10; RRID:AB_2145209	IF(1:200)
recombinant DNA reagent	pCAGG (plasmid)	Krispin et al., 2010b DOI:10.1242/dev.041509		
recombinant DNA reagent	pCAGGS-EGFP (plasmid)	Krispin et al., 2010b DOI:10.1242/dev.041509		
recombinant DNA reagent	pCAG-mGFP (plasmid)	Addgene	RRID:Addgene_14757	
recombinant DNA reagent	pCAGGS-RFP (plasmid)	Ofek et al., 2021 DOI:10.1186/s12915-021-01014-3		
recombinant DNA reagent	pCAGGS-RARα403 (plasmid)	This paper		Subcloned as described in Methods section
recombinant DNA reagent	pCAGGS-Cyp26A1 (plasmid)	This paper		Subcloned as described in Methods section
recombinant DNA reagent	pCAB-cSmad6 (plasmid)	Nitzan et al., 2016 DOI:10.1186/s12915-016-0245-6		
recombinant DNA reagent	pCAG-VP16-RARα-IRES-eGFP (plasmid)	Novitch et. 2003 DOI:10.1016/j.neuron.2003.08.006		From S. Sockanathan

recombinant DNA reagent	pGL3-RARE-SV40-AP (plasmid)	Gupta and Sen, 2015 DOI:10.1242/dev.122390		From J. Sen
recombinant DNA reagent	pGL3-RARE-SV40-RFP (plasmid)	This paper		Subcloned as described in Methods section
recombinant DNA reagent	pGL3-RARE-SV40-d2EGFP (plasmid)	This paper		Subcloned as described in Methods section
recombinant DNA reagent	12XTOPFLASH-d2EGFP (plasmid)	Rios et al., 2010 DOI:10.1002/dvdy.22174		
recombinant DNA reagent	c*Raldh2* (plasmid)	Del Corral et al., 2003 DOI:10.1016/s0896-6273(03)00565-8		From K. Storey Template for probe synthesis
recombinant DNA reagent	c*BAMBI* (plasmid)	Casanova et al., 2012 DOI:10.1371/journal.pone.0052781	EST 603482731F1	From A. Sanz-Ezquerro Template for probe synthesis
recombinant DNA reagent	c*Cyp26A1* (plasmid)	Wilson et al., 2007 DOI:10.1016/j.ydbio.2004.01.034		From R. Wingate Template for probe synthesis
recombinant DNA reagent	c*Hairy1* (plasmid)	Jouve et al., 2000; Nitzan et al., 2016 DOI:10.1242/dev.127.7.1421 DOI:10.1186/s12915-016-0245-6		From D. Henrique Template for probe synthesis
recombinant DNA reagent	c*foxd3* (plasmid)	Dottori et al., 2001 DOI:10.1242/dev.128.21.4127	EST 603374321F1	From M. Cheung Template for probe synthesis
recombinant DNA reagent	c*RARα* (plasmid)	Del Corral et al., 2003		From K. Storey Template for probe synthesis

		DOI:10.1016/s0896-6273(03)00565-8		
recombinant DNA reagent	c*RARβ* (plasmid)	Del Corral et al., 2003 DOI:10.1016/s0896-6273(03)00565-8		From K. Storey Template for probe synthesis
recombinant DNA reagent	c*RARγ* (plasmid)	A. Graham		Template for probe synthesis
recombinant DNA reagent	c*RXRα* (plasmid)	A. Graham		Template for probe synthesis
recombinant DNA reagent	c*RXRγ* (plasmid)	A. Graham		Template for probe synthesis
sequence-based reagent	q*Cyp1B1*_F	This paper	PCR primers	GTGTTGTGACTGCTGGGATG
sequence-based reagent	q*Cyp1B1*_R	This paper	PCR primers	AGATTGACCAGTGAGCCAGG
sequence-based reagent	q*sox9*_F	This paper	PCR primers	TCGAAGGAAACTGGCTGACC
sequence-based reagent	q*sox9*_R	This paper	PCR primers	ATCAATGTGGGGAGGTTGGC
sequence-based reagent	q*Rspo1*_F	This paper	PCR primers	AAACCACCGGTCTCTGTGTC
sequence-based reagent	q*Rspo1*_R	This paper	PCR primers	AGCAGGAGGGAAGGAAGAAG
sequence-based reagent	q*draxin*_F	This paper	PCR primers	TGTGCTGGATGTGGTTGTTT
sequence-based reagent	q*draxin*_R	This paper	PCR primers	TGGTTTGCAGAGATGCTCAC
sequence-based reagent	q*Grem1*_F	This paper	PCR primers	AGGCTGCTTTTGGAGAACAA
sequence-based reagent	q*Grem1*_R	This paper	PCR primers	GAATGGGTTTTGGTTGATG

sequence-based reagent	q*CRABP1*_F	This paper	PCR primers	ACCTGGAAGATGAGGAGCAG
sequence-based reagent	q*CRABP1*_R	This paper	PCR primers	CACACGGTCACATACAACACC
sequence-based reagent	*qNorrin(NDP)*_F	This paper	PCR primers	GCACTGTCCTAAAGCAGCCT
sequence-based reagent	q*Norrin(NDP)*_R	This paper	PCR primers	TTCAGGCCCCGGGAGATATT
sequence-based reagent	q*snai2*_F	This paper	PCR primers	TGAGATACGGGGAAAGACGC
sequence-based reagent	q*snai2*_R	This paper	PCR primers	AGGCACTTGGAGGGGTAATG
commercial assay or kit	KAPA2G Fast ReadyMix PCR	Sigma Israel	Cat#KK5101	
chemical compound, drug	NBT	Roche	Cat#11383213001	
chemical compound, drug	BCIP	Sigma Israel	Cat#B8503	
chemical compound, drug	Fast Red	Sigma Israel	Cat#F4648	
software, algorithm	FIJI	Schindelin et al., 2009	https://imagej.net/software/fiji/	
software, algorithm	R and R-Studio		https://www.R-project.org; http://www.rstudio.com	
software, algorithm	Adobe Photoshop and Indesign CS6	Adobe	https://www.adobe.com/	
software, algorithm	Graphpad Prism 7.0	Graphpad	https://www.graphpad.com	

other	BTX square wave electroporator	BTX, San Diego, CA, USA	Cat#45-0662	
other	DP73 cooled CCD digital camera	Olympus	https://www.olympus-global.com/	
other	BX51 microscope	Olympus	https://www.olympus-global.com/	
other	Nikon Eclipse 90i microscope	Nikon	https://www.nikon.com/	
other	D-Eclipse c1 confocal system	Nikon	https://www.nikon.com/	
other	DIG RNA mix	Roche	Cat#11277073910	
other	anti-digoxigenin-AP	Roche	Cat#11093274910	
other	Hoechst 33258 stain	Sigma Israel	Cat#14530	(125 ng/ml)

785

Embryos

Fertilized quail (*Coturnix coturnix Japonica*) eggs were obtained from commercial sources (Moshav Mata), kept at 15°C and then incubated at 38 °C to desired stages. Embryos were staged by the number of somite pairs formed (somite stage – ss). All experiments were conducted at the flank level of the axis.

Expression vectors and *in ovo* electroporation

The following expression vectors were used as controls: pCAGG, pCAGGS-EGFP (Krispin et al., 2010b), pCAG-mGFP (Addgene #14757), pCAGGS-RFP (Ofek et al., 2021). PCAGGS-RARα403 and PCAGGS-Cyp26A1 (subcloned from PCAGGS-RARα403-IRES-eGFP and PCAGGS-Cyp26A1-IRES-eGFP, respectively, from S. Sockanathan (Novitch et al., 2003), were applied to inhibit RA activity. pCAB-cSmad6 was implemented to inhibit BMP activity (Nitzan et al., 2016). pCAG-VP16-RARα-IRES-eGFP was used to activate RA activity (Novitch et al., 2003).

To monitor RA activity, we used the pGL3-RARE-SV40-AP reporter [from J. Sen, (Gupta and Sen, 2015)]. Fluorescent versions of this reporter were prepared by replacing the AP tag with either RFP or with a destabilized version of GFP (pGL3-RARE-SV40-RFP and pGL3-RARE-SV40-d2EGFP, respectively (Clontech). Wnt activity was measured with 12XTOPFLASH-d2EGFP (Rios et al., 2010).

Unilateral, bilateral and/or double electroporations to the NT were performed as detailed under Results. To this end, DNA (4 ug/ul) was mixed with Fast Green and microinjected into the lumen of the NT at the flank level of the axis. Five mm tungsten electrodes were placed on

either side of the embryo. A square wave electroporator (BTX, San Diego, CA, USA) was used to deliver one pulse of current at 17–25 V for 6 ms.

Mechanical separation of the paraxial mesoderm from the NT

A unilateral slit between epithelial somites and NT comprising an approximate length of 8 segments was performed. A piece of aluminum foil was then inserted that extended beyond the dorsal border of the tissues to provide a continuous barrier despite embryo growth. In some cases, the dorsal NT was additionally opened to separate between both halves of the neuroepithelium. Following microsurgery, embryos were reincubated for 48 hours prior to fixation.

Immunohistochemistry

For immunostaining, embryos were fixed overnight at 4 °C with 4% formaldehyde (PFA) in phosphate-buffered saline (PBS) (pH 7.4), embedded in paraffin wax and serially sectioned at 8 μm. Immunostaining was performed either on whole mount embryos or on paraffin sections, as previously described (Burstyn-Cohen and Kalcheim, 2002; Kahane and Kalcheim, 2020). Antibodies were diluted in PBS containing 5% fetal bovine serum (Biological Industries Israel, 04-007-1A) and 1% or 0.1% Triton X-100 (Sigma Aldrich Israel, X-100), respectively. Antibodies used were: rabbit anti-GFP (1:1000, Invitrogen, Thermo-Fisher Scientific, A-6455), mouse anti-GFP (1:100, Abcam, Ab38689), rabbit anti-RFP (1:1000, OriGene, AP09229PU-N), guinea pig anti-pSmad1/5/8 (1:300, a gift from E. Laufer), mouse anti-H3-pS10 (1:400, Abcam, Ab14955), rabbit anti-Laminin (1:100, Sigma Israel, L9393), rabbit anti-Sox9 (1:150, Millipore, AB5535), rabbit anti-SNAI2 (1:500; Cell Signaling Technologies,

9585), mouse anti-CD57 (anti-HNK1, 1:500, BD Biosciences, 559048), rabbit anti-BarHL1 (1:300, Sigma Israel, HPA004809), mouse anti-Pax7 (1:10, DHSB, pax7), mouse anti-Hb9 (1:200, DHSB, 81.5C10). Cell nuclei were visualized with 125 ng/ml Hoechst 33258 (Sigma Israel, 14530) diluted in PBS.

In-situ hybridization

For *in-situ* hybridization (ISH), embryos were fixed with Fornoy (60% ethanol, 30% formaldehyde and 10% acetic acid) for 1 hour at room temperature, embedded in paraffin wax and serially sectioned at 10 μm. ISH was performed on sections. In brief, sections were treated with 1 ug/ml proteinase K, refixed in 4% PFA, then hybridized overnight at 65 °C with digoxigenin-labeled RNA probes (Roche, 11277073910). The probes were detected with AP coupled with anti-digoxigenin Fab fragments (Roche, 11093274910). AP reaction was developed with 4-Nitro blue tetrazolium chloride (NBT, Roche, 11383213001) and 5-bromo-4-chloro-3'-indolyphosphate p-toluidine salt (BCIP, Sigma Israel, B8503). In the *foxd3/Rspo1* ISH experiment, the AP reaction of *Rspo1* was developed with Fast Red (Sigma Israel, F4648) for 2 hours at room temperature. Importantly, all hybridizations, whether done on intact embryos at NC vs. RP stages, or in control vs. experimental embryos, were always developed for the same time per given probe and experiment. The RNA probes used are described in the Key Resources Table. Several probes were produced by PCR amplification (KAPA2G Fast ReadyMix PCR kit, Sigma Israel, KK5101). cDNA templates were synthesized by RNA precipitation followed by reverse transcription PCR. RNAs were produced from 20ss-E4 quail embryos. Tissue samples were homogenized with TriFast reagent, and RNA was separated with chloroform and isopropanol. The primers used are depicted in Key Resources Table.

Data acquisition and statistical analysis

Measurement of the intensity of immunofluorescence and ISH signals: Intensities were measured using FIJI (Schindelin et al., 2009). In most cases, the RP was selected as the region of interest (ROI); mean intensity was measured and background intensity was then subtracted. Average intensity of all sections was calculated per embryo, and values were normalized with a control mean set as 1.

For measurement of phospho-Smad1/5/9 intensity, the ROI was selected as the dorsal domain of the NT from the dorsal midline to the ventral border of dI1 progenitors.

To monitor intensity of laminin immunostaining in the RP basal lamina, a segmented line of width 4 was drawn along the basal aspect of the RP, and mean intensity was measured within that area. Average intensity was calculated for each embryo and expressed relative to a control value set as 1.

To measure the relative position of cell nuclei across the apico-basal extent of the RP, the latter was divided into basal and apical halves, and Hoechst-stained nuclei were manually counted in both domains.

The distance of BarHL1^{+} cells from the dorsal midline of the NT was measured for each cell manually using FIJI, and histograms were generated using R (https://www.R-project.org/) in Rstudio (http://www.rstudio.com/).

Images were photographed using a DP73 (Olympus) cooled CCD digital camera mounted on a BX51 microscope (Olympus) with Uplan FL-N 20x/0.5 and 40x/0.75 dry objectives (Olympus). Confocal sections encompassing their entire thickness were photographed using a Nikon Eclipse 90i microscope with a Plan Apo 40x/1.3 or 100x/1.4 objectives (Nikon) and a

D-Eclipse c1 confocal system (Nikon) at 1.0 μm increments through the z-axis. Images were z-stacked with FIJI software.

For quantification, images of control and treated sections were photographed under the same conditions. For figure preparation, images were exported into Photoshop CS6 (Adobe). If necessary, the levels of brightness and contrast were adjusted to the entire image and images were cropped without color correction adjustments or γ adjustments. Graphics were generated using Graphpad Prism 7.0, and figures were prepared using Photoshop and InDesign CS6.

Results were processed with Graphpad Prism 7 and presented as scatter plots with mean±SEM. Data were subjected to statistical analysis using either of the following tests, as described in the respective legends to Figures: Student's t-test, Welch's t-test, Mann-Whitney test, 1-way ANOVA with post-hoc Tukey test, Kruskal-Wallis with post-hoc Dunn's test and Wilcoxon signed ranks test. All tests applied were two-tailed and a P-value ≤ 0.05 was considered significant.

Acknowledgments

We are grateful to all the researchers whose names are mentioned along the text for generously providing reagents. We thank Avihu Klar and Joel Yisraeli for critical reading of the manuscript. This study was supported by grants from the Israel Science Foundation (ISF #209/18) and from the Ines Mandl Research Fund (IMRF) to CK.

Author Contributions

DR and CK conceived the article, wrote it and prepared the Figures. DR performed the experiments. Both authors discussed and agreed on the text and approved the manuscript.

Conflicts of Interest

The authors declare no conflict of interests

902 **References**

903 **Andrews, M. G., Kong, J., Novitch, B. G. and Butler, S. J.** (2019). New perspectives on
904 the mechanisms establishing the dorsal-ventral axis of the spinal cord. *Curr Top Dev*
905 *Biol* **132**, 417–450.

906 **Augsburger, A., Schuchardt, A., Hoskins, S., Dodd, J. and Butler, S.** (1999). Bmps as
907 mediators of roof plate repulsion of commissural neurons. *Neuron* **24**, 127–141.

908 **Berggren, K., McCaffery, P., Drager, U. and Forehand, C. J.** (1999). Differential
909 distribution of retinoic acid synthesis in the chicken embryo as determined by
910 immunolocalization of the retinoic acid synthetic enzyme, RALDH-2. *Dev Biol* **210**,
911 288–304.

912 **Blentic, A., Gale, E. and Maden, M.** (2003). Retinoic acid signalling centres in the avian
913 embryo identified by sites of expression of synthesising and catabolising enzymes. *Dev*
914 *Dyn* **227**, 114–127.

915 **Brazil, D. P., Church, R. H., Surae, S., Godson, C. and Martin, F.** (2015). BMP
916 signalling: agony and antagony in the family. *Trends Cell Biol* **25**, 249–264.

917 **Bronner-Fraser, M. and Fraser, S. E.** (1988). Cell lineage analysis reveals multipotency of
918 some avian neural crest cells. *Nature* **335**, 161–164.

919 **Bronner, M. E.** (2012). Formation and migration of neural crest cells in the vertebrate
920 embryo. *Histochem Cell Biol* **138**, 179–186.

921 **Burstyn-Cohen, T. and Kalcheim, C.** (2002). Association between the cell cycle and neural
922 crest delamination through specific regulation of G1/S transition. *Dev. Cell* **3**,.

923 **Burstyn-Cohen, T., Stanleigh, J., Sela-Donenfeld, D. and Kalcheim, C.** (2004). Canonical
924 Wnt activity regulates trunk neural crest delamination linking BMP/noggin signaling

925 with G1/S transition. *Development* **131**, 5327–5339.

926 **Butler, S. J. and Dodd, J.** (2003). A role for BMP heterodimers in roof plate-mediated
927 repulsion of commissural axons. *Neuron* **38**, 389–401.

928 **Castillo, H. A., Cravo, R. M., Azambuja, A. P., Simões-Costa, M. S., Sura-Trueba, S.,**
929 **Gonzalez, J., Slonimsky, E., Almeida, K., Abreu, J. G., Afonso de Almeida, M. A.,**
930 **et al.** (2010). Insights into the organization of dorsal spinal cord pathways from an
931 evolutionarily conserved raldh2 intronic enhancer. *Development* **137**, 507–518.

932 **Chambers, D., Wilson, L., Maden, M. and Lumsden, A.** (2007). RALDH-independent
933 generation of retinoic acid during vertebrate embryogenesis by CYP1B1. *Development*
934 **134**, 1369–1383.

935 **Chesnutt, C., Burrus, L. W., Brown, A. M. and Niswander, L.** (2004). Coordinate
936 regulation of neural tube patterning and proliferation by TGFbeta and WNT activity.
937 *Dev Biol* **274**, 334–347.

938 **Chizhikov, V. V and Millen, K. J.** (2005). Roof plate-dependent patterning of the vertebrate
939 dorsal central nervous system. *Dev Biol* **277**, 287–295.

940 **Despin-Guitard, E. and Migeotte, I.** (2021). Mitosis , a springboard for epithelial-
941 mesenchymal transition ? *Cell Cycle* **20**, 2452–2464.

942 **Diez del Corral, R. and Morales, A. V.** (2014). Retinoic acid signaling during early spinal
943 cord development. *J. Dev. Biol.* **2**, 174–197.

944 **Diez del Corral, R., Olivera-Martinez, I., Goriely, A., Gale, E., Maden, M. and Storey,**
945 **K.** (2003). Opposing FGF and retinoid pathways control ventral neural pattern, neuronal
946 differentiation, and segmentation during body axis extension. *Neuron* **40**, 65–79.

947 **Duval, N., Vaslin, C., Barata, T. C., Frarma, Y., Contremoulins, V., Baudin, X.,**

948 **Nedelec, S. and Ribes, V. C.** (2019). BMP4 patterns Smad activity and generates
949 stereotyped cell fate organization in spinal organoids. *Development* **146**, doi:
950 10.1242/dev.175430.

951 **Endo Y., Osumi N. and Wakamatsu Y.** (2003). Bimodal functions of Notch-mediated
952 signaling are involved in neural crest formation during avian ectoderm development.
953 *Development.* **129**, 863–873.

954 **George, L., Chaverra, M., Todd, V., Lansford, R. and Lefcort, F.** (2007). Nociceptive
955 sensory neurons derive from contralaterally migrating, fate-restricted neural crest cells.
956 *Nat Neurosci* **10**, 1287–1293.

957 **Gupta, S. and Sen, J.** (2015). Retinoic acid signaling regulates development of the dorsal
958 forebrain midline and the choroid plexus in the chick. *Dev.* **142**, 1293–1298.

959 **Halperin-Barlev, O. and Kalcheim, C.** (2011). Sclerotome-derived slit1 drives directional
960 migration and differentiation of robo2-expressing pioneer myoblasts. *Development* **138**,.

961 **Haselbeck, R. J., Hoffmann, I. and Duester, G.** (1999). Distinct functions for Aldh1 and
962 Raldh2 in the control of ligand production for embryonic retinoid signaling pathways.
963 *Dev. Genet.* **25**, 353–364.

964 **Hegarty, S. V., O'Keeffe, G. W. and Sullivan, A. M.** (2013). BMP-Smad 1/5/8 signalling
965 in the development of the nervous system. *Prog. Neurobiol.* **109**, 28–41.

966 **Helms, A. W. and Johnson, J. E.** (2003). Specification of dorsal spinal cord interneurons.
967 *Curr Opin Neurobiol* **13**, 42–49.

968 **Holguera, I. and Desplan, C.** (2018). Neuronal specification in space and time. *Science (80-.*
969 *).* **362**, 176–180.

970 **Isabella, A. J., Barsh, G. R., Stonick, J. A., Dubrulle, J. and Moens, C. B.** (2020).

Retinoic Acid Organizes the Zebrafish Vagus Motor Topographic Map via Spatiotemporal Coordination of Hgf/Met Signaling. *Dev. Cell* **53**, 344-357.e5.

Kahane, N. and Kalcheim, C. (1998). Identification of early postmitotic cells in distinct embryonic sites and their possible roles in morphogenesis. *Cell Tissue Res.* **294**, 297–307.

Kahane, N. and Kalcheim, C. (2020). Neural tube development depends on notochord-derived sonic hedgehog released into the sclerotome. *Development* **147**,.

Kalcheim, C. (2018). Neural crest emigration: From start to stop. *Genesis* **56**,.

Kalcheim, C. and Kumar, D. (2017). Cell fate decisions during neural crest ontogeny. *Int. J. Dev. Biol.* **61**, 195–203.

Kam, R. K. T., Deng, Y., Chen, Y. and Zhao, H. (2012). Retinoic acid synthesis and functions in early embryonic development. *Cell Biosci.* **2**, 11.

Kidd, T., Bland, K. S. and Goodman, C. S. (1999). Slit is the midline repellent for the robo receptor in Drosophila. *Cell* **96**, 785–794.

Kohwi, M. and Doe, C. Q. (2013). Temporal fate specification and neural progenitor competence during development. *Nat. Rev. Neurosci.* **14**, 823–838.

Krispin, S., Nitzan, E. and Kalcheim, C. (2010a). The dorsal neural tube: A dynamic setting for cell fate decisions. *Dev. Neurobiol.* **70**,.

Krispin, S., Nitzan, E., Kassem, Y. and Kalcheim, C. (2010b). Evidence for a dynamic spatiotemporal fate map and early fate restrictions of premigratory avian neural crest. *Development* **137**, 585–595.

Kukreja, S., Udaykumar, N., Yogesh, B. and Sen, J. (2020). Retinoic acid signaling

993 regulates proliferation and lamina formation in the developing chick optic tectum. *Dev.*
994 *Biol.* **467**, 95–107.

995 **Lara-Ramírez, R., Zieger, E. and Schubert, M.** (2013). Retinoic acid signaling in spinal
996 cord development. *Int. J. Biochem. Cell Biol.* **45**, 1302–1313.

997 **Le Douarin, N. M. and Kalcheim, C.** (1999). *The Neural Crest*. 2nd ed. New York:
998 Cambridge University Press.

999 **Le Dréau, G. and Martí, E.** (2013). The multiple activities of BMPs during spinal cord
1000 development. *Cell. Mol. Life Sci.* **70**, 4293–4305.

1001 **Lee, K. J., Mendelsohn, M. and Jessell, T. M.** (1998). Neuronal patterning by BMPs: a
1002 requirement for GDF7 in the generation of a discrete class of commissural interneurons
1003 in the mouse spinal cord. *Genes Dev.* **12**, 3394–3407.

1004 **Maden, M., Ong, D. E., Summerbell, D., Chytil, F. and Hirst, E. A.** (1989). Cellular
1005 retinoic acid-binding protein and the role of retinoic acid in the development of the chick
1006 embryo. *Dev. Biol.* **135**, 124–132.

1007 **Martinez-Morales, P. L., Diez del Corral, R., Olivera-Martinez, I., Quiroga, A. C., Das,**
1008 **R. M., Barbas, J. A., Storey, K. G. and Morales, A. V** (2011). FGF and retinoic acid
1009 activity gradients control the timing of neural crest cell emigration in the trunk. *J Cell*
1010 *Biol* **194**, 489–503.

1011 **Martínez-Morales, P. L., del Corral, R. D., Olivera-Martínez, I., Quiroga, A. C., Das, R.**
1012 **M., Barbas, J. A., Storey, K. G. and Morales, A. V.** (2011). FGF and retinoic acid
1013 activity gradients control the timing of neural crest cell emigration in the trunk. *J. Cell*
1014 *Biol.* **194**, 489–503.

1015 **Muroyama, Y., Fujihara, M., Ikeya, M., Kondoh, H. and Takada, S.** (2002). Wnt

1016 signaling plays an essential role in neuronal specification of the dorsal spinal cord.
1017 *Genes Dev.* **16**, 548–553.

1018 **Niederreither, K., Subbarayan, V., Dollé, P. and Chambon, P.** (1999). Embryonic retinoic
1019 acid synthesis is essential for early mouse post- implantation development. *Nat. Genet.*
1020 **21**, 444–448.

1021 **Nieto, M. A., Sargent, M. G., Wilkinson, D. G. and Cooke, J.** (1994). Control of cell
1022 behavior during vertebrate development by slug, a zinc finger gene. *Science (80-.).* **264**,
1023 835–839.

1024 **Nitzan, E., Krispin, S., Pfaltzgraff, E. R., Klar, A., Labosky, P. A. and Kalcheim, C.**
1025 (2012). A dynamic code of dorsal neural tube genes regulates the segregation between
1026 neurogenic and melanogenic neural crest cells. *Dev.* **140**,.

1027 **Nitzan, E., Avraham, O., Kahane, N., Ofek, S., Kumar, D. and Kalcheim, C.** (2016).
1028 Dynamics of BMP and Hes1/Hairy1 signaling in the dorsal neural tube underlies the
1029 transition from neural crest to definitive roof plate. *BMC Biol.* **14**, 23. DOI
1030 10.1186/s12915-016-0245–6.

1031 **Novitch, B. G., Wichterle, H., Jessell, T. M. and Sockanathan, S.** (2003). A requirement
1032 for retinoic acid-mediated transcriptional activation in ventral neural patterning and
1033 motor neuron specification. *Neuron* **40**, 81–95.

1034 **Ofek, S., Wiszniak, S., Kagan, S., Tondl, M., Schwarz, Q. and Kalcheim, C.** (2021).
1035 Notch signaling is a critical initiator of roof plate formation as revealed by the use of
1036 RNA profiling of the dorsal neural tube. *BMC Biol.* **19:84**,
1037 https://doi.org/10.1186/s12915-021-01014-3.

1038 **Reijntjes, S., Blentic, A., Gale, E. and Maden, M.** (2005). The control of morphogen

1039 signalling: regulation of the synthesis and catabolism of retinoic acid in the developing
1040 embryo. *Dev Biol* **285**, 224–237.

1041 **Rekler, D. and Kalcheim, C.** (2021). From Neural Crest to Definitive Roof Plate : The
1042 Dynamic Behavior of the Dorsal Neural Tube. *Int. J. Mol. Sci.* **22**, 3911.

1043 **Rhinn, M. and Dollé, P.** (2012). Retinoic acid signalling during development. *Development*
1044 **139**, 843–858.

1045 **Rios, A. C., Denans, N. and Marcelle, C.** (2010). Real-time observation of Wnt beta-catenin
1046 signaling in the chick embryo. *Dev Dyn* **239**, 346–353.

1047 **Schindelin, J., Arganda-Carrera, I., Frise, E., Verena, K., Mark, L., Tobias, P., Stephan,**
1048 **P., Curtis, R., Stephan, S., Benjamin, S., et al.** (2009). Fiji - an Open platform for
1049 biological image analysis. *Nat. Methods* **9**,.

1050 **Sela-Donenfeld, D. and Kalcheim, C.** (1999). Regulation of the onset of neural crest
1051 migration by coordinated activity of BMP4 and Noggin in the dorsal neural tube.
1052 *Development* **126**, 4749–4762.

1053 **Sela-Donenfeld, D. and Kalcheim, C.** (2002). Localized BMP4-noggin interactions generate
1054 the dynamic patterning of noggin expression in somites. *Dev. Biol.* **246**,.

1055 **Shaker, M. R., Lee, J., Park, S., Kim, J. Y., Son, G. H., Son, J. W., Park, B. H., Rhyu, I.**
1056 **J., Kim, H. and Sun, W.** (2020). Stem Cell Reports. *Stem Cell Reports* **15**, 1–14.

1057 **Sheng, N., Xie, Z., Wang, C., Bai, G., Zhang, K., Zhu, Q., Song, J., Guillemot, F., Chen,**
1058 **Y. G., Lin, A., et al.** (2010). Retinoic acid regulates bone morphogenic protein signal
1059 duration by promoting the degradation of phosphorylated Smad1. *Proc. Natl. Acad. Sci.*
1060 *U. S. A.* **107**, 18886–18891.

1061 **Shinozuka, T., Takada, R., Yoshida, S., Yonemura, S. and Takada, S.** (2019). Wnt

1062 produced by stretched roof-plate cells is required for the promotion of cell proliferation
1063 around the central canal of the spinal cord. *Development* **146**,.

1064 **Sun, J., Zhuang, F. F., Mullersman, J. E., Chen, H., Robertson, E. J., Warburton, D.,**
1065 **Liu, Y. H. and Shi, W.** (2006). BMP4 activation and secretion are negatively regulated
1066 by an intracellular Gremlin-BMP4 interaction. *J. Biol. Chem.* **281**, 29349–29356.

1067 **Theveneau, E. and Mayor, R.** (2012a). Neural crest delamination and migration: from
1068 epithelium-to-mesenchyme transition to collective cell migration. *Dev Biol* **366**, 34–54.

1069 **Theveneau, E. and Mayor, R.** (2012b). Neural crest migration: interplay between
1070 chemorepellents, chemoattractants, contact inhibition, epithelial-mesenchymal
1071 transition, and collective cell migration. *Wiley Interdiscip Rev Dev Biol* **1**, 435–445.

1072 **Timmer, J. R., Wang, C. and Niswander, L.** (2002). BMP signaling patterns the dorsal and
1073 intermediate neural tube via regulation of homeobox and helix-loop-helix transcription
1074 factors. *Development* **129**, 2459–2472.

1075 **Tozer, S., Le Dreau, G., Marti, E. and Briscoe, J.** (2013). Temporal control of BMP
1076 signalling determines neuronal subtype identity in the dorsal neural tube. *Development*
1077 **140**, 1467–1474.

1078 **Venepally, P., Reddy, L. G. and Sani, B. P.** (1996). Characterization of cellular retinoic
1079 acid-binding protein I from chick embryo and its ligand binding properties.
1080 *Arch.Biochem.Biophys.* **336**, 231–239.

1081 **Wilson, L., Gale, E., Chambers, D. and Maden, M.** (2004). Retinoic acid and the control
1082 of dorsoventral patterning in the avian spinal cord. *Dev Biol* **269**, 433–446.

1083 **Wine-Lee, L., Ahn, K. J., Richardson, R. D., Mishina, Y., Lyons, K. M. and Crenshaw,**
1084 **E. B.** (2004). Signaling through BMP type 1 receptors is required for development of

1085 interneuron cell types in the dorsal spinal cord. *Development* **131**, 5393–5403.

1086 **Xing, L., Anbarchian, T., Tsai, J. M., Plant, G. W. and Nusse, R.** (2018). Wnt/beta-
1087 catenin signaling regulates ependymal cell development and adult homeostasis. *Proc*
1088 *Natl Acad Sci U S A* **115**, E5954–E5962.

1089 **Zechner, D., Muller, T., Wende, H., Walther, I., Taketo, M. M., Crenshaw 3rd, E. B.,**
1090 **Treier, M., Birchmeier, W. and Birchmeier, C.** (2007). Bmp and Wnt/beta-catenin
1091 signals control expression of the transcription factor Olig3 and the specification of spinal
1092 cord neurons. *Dev Biol* **303**, 181–190.

1093

1094